A thermo-viscoplastic constitutive model for **FCC** metals with application to OFHC copper

A. Rusinek [a,*], J.A. Rodríguez-Martínez [b], A. Arias [b]

[a] National Engineering School of Metz (ENIM), Laboratory of Mechanic, Biomechanics, Polymers and Structures (LABPS), Ile du Saulcy, 57000 Metz, France
[b] Department of Continuum Mechanics and Structural Analysis, University Carlos III of Madrid, Avda. de la Universidad 30, 28911 Leganés, Madrid, Spain

ARTICLE INFO

ABSTRACT

In this paper a physical based constitutive relation for defining the thermo viscoplastic behaviour of **FCC** metals with dependence on strain on thermal activation processes is presented. The model, based on previous considerations reported by Rusinek and Klepaczko [Rusinek A, Klepaczko JR. Shear testing of sheet steel at wide range of strain rates and a constitutive relation with strain rate and temperature dependence of the flow stress. Int J Plasticity 2001;17:87 115], is founded on physical aspects of the material behaviour. The proposed constitutive relation is applied to define the behaviour of oxygen free high conductivity (OFHC) copper using the experimental data reported in Nemat Nasser and Li [Nemat Nasser S, Li Y. Flow stress of FCC polycrystals with application to OFHC copper. Acta Mater 1998;46:565 77]. The description of the material behaviour provided by the model gets satisfactory agreement with the experiments. The analytical predictions of this constitutive description are compared with those obtained from the models due to Voyiadjis and Almasri [Voyiadjis GZ, Almasri AH. A physically based constitutive model for fcc metals with applications to dynamic hardness. Mech Mater 2008;40:549 63], and Nemat Nasser and Li. This comparison reveals that the original formulation proposed in this paper is a suitable alternative to other physically based relations for modeling OFHC copper.

1. Introduction

Over the last decades, deformation of metals has been subjected to intensive study since it is of fundamental interest to analyze loading processes. Accurate knowledge of the response of metallic alloys under loading is required to optimize materials used to build mechanical elements in charge of bearing demand ing solicitations. In order to understand the thermo viscoplastic behaviour of metals, a constitutive description is required. Driven by economic sectors like automotive, aeronautical or military industries, the research conducted to derive theoretical descrip tions of the deformation behaviour of metallic alloys has gathered substantial efforts.

Macroscopic constitutive descriptions proposed over the years may be primarily split into two groups:

- *Phenomenological constitutive relations*: They provide a defini tion of the material flow stress based on empirical observa tions. They consist of mathematical functions with lack of physical background that fit experimental observations. Phe nomenological models are characterized by reduced number of material constants and easy calibration. Some examples are those models proposed in [1 5]. Due to their empirical character, they are used in restricted application fields (*cover ing limited ranges of strain rate and temperature*) and they exhibit reduced flexibility (*specific formulation for determined materials*).

- *Physical based constitutive relations*: They account for physical aspects of the material behaviour. Most of them are founded on the theory of thermodynamics and kinetics of slips developed in [6]. Some examples are those models proposed in [7 17]. In comparison with phenomenological descriptions they use a larger number of material constants and their determination procedure follows physical assumptions. In contrast, they allow for an accurate definition of material behaviours under wide ranges of loading conditions.

In the present work, our attention will be focused on the second sort of constitutive relations previously mentioned. Due to their flexibility, physical based models are of increasing interest for engineering applications like high speed machining (**HSM**), perforation or crash test [18]. During such processes, the material work piece is subjected to wide ranges of strain rate and temperature as well as large deformations [18].

* Corresponding author. Tel.: +33 3 87 34 69 30; fax: +33 3 87 34 42 79.
 E-mail address: rusinek@enim.fr (A. Rusinek).

2. Theoretical considerations

Macroscopic plasticity in metals is the result of dislocations moving through the crystal lattice. Two types of obstacles are encountered that try to prevent dislocation movements through the lattice: long range and short range barriers [6,12,15,19 21]. Long range obstacles are due to the structure of the material and cannot be overcome by introducing thermal energy through the crystal [7,8,22]. They contribute to the flow stress with a component that is non thermally activated (*athermal stress*). Overcoming of short range barriers can be assisted by thermal energy [7,8,15,21,22]. Thermal activation aids dislocation gliding, decreasing the intrinsic lattice friction in the case of **BBC** metals (*overcoming Peierls stress*) or decreasing the strength of obstacles in the case of **FCC** metals (*overcoming forests of dislocations*). In both cases, thermal activation reduces the applied stress required to force the dislocation past obstacles [23].

Thus, flow stress of a material (*using J2 theory*) can be decomposed into equivalent athermal stress $\overline{\sigma}_\mu$ and equivalent thermal stress $\overline{\sigma}^*$ [7,13,15,19,22,24 26]:

$$\overline{\sigma} = \overline{\sigma}_\mu + \overline{\sigma}^* \tag{1}$$

A scheme of the evolution of stress components along with temperature is depicted in Fig. 1. At low temperature, flow stress decreases with temperature. This region is influenced by thermal and athermal stress components. The next region with increasing temperature is basically athermal. At very high temperature, flow stress decreases again with increasing temperature. According to the considerations reported, for example in [15], it must be pointed out that it is not necessary for all metals to have the three regions described here.

Definition (*and contribution to the overall flow stress*) of thermal and athermal terms is dependent on the crystal structure of the material. The causes are related to available symmetries of the lattice, the nature of dislocation cores and the available slip systems as reported in [23].

In **BCC** metals, overcoming Peierls stress resistance is the main phenomenon involved in thermally activated processes [27]. Consequently, the thermal component of the flow stress $\overline{\sigma}^* = \overline{\sigma}^*(\dot{\overline{\varepsilon}}^p, T)|_{BCC}$ can be defined independent of plastic strain [7,9,10]. The yield stress of most **BCC** metals is strongly temperature and rate dependent [7,12,28,29]. Strain hardening is primarily accomplished through long range barriers [6] such as grain boundaries, far field forest of dislocations and other microstructural elements with far field influence [8]. Temperature and deformation rate have relatively small effect on strain hardening (Fig. 2).
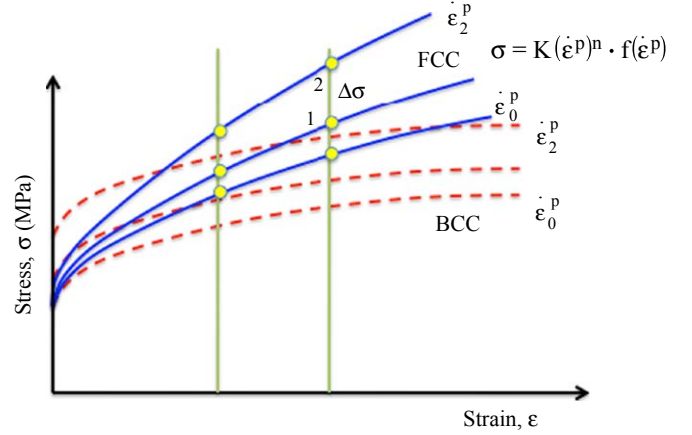

Fig. 1. Decomposition of macroscopic stress versus temperature.

Fig. 2. Strain rate sensitivity definition for **BCC** and **FCC** metals.

Peierls stress in many **FCC** metals is relatively unimportant [12,23]. The rate controlling mechanism is the overcoming of dislocation forests by individual dislocations [12]. Thermal activation behaviour becomes dependent on the plastic strain $\overline{\sigma}^* = \overline{\sigma}^*(\overline{\varepsilon}^p, \dot{\overline{\varepsilon}}^p, T)|_{FCC}$ [7,8,12,23]. **FCC** metals exhibit large strain hardening due to an increase in the amount of dislocation interactions with increasing strain [23]. Strain hardening tends to be highly temperature and strain rate dependent, while the yield stress has reduced dependence on such effects [23] (Fig. 2).

In agreement with previous considerations, the volume thermally activated (**VTA**) defined by Eq. (2) [30,31] decreases with plastic strain for many **FCC** metals [7,15,32] while it is independent of the deformation level for **BCC** metals [15,33].

$$V^* \approx kT \frac{\partial \ln(\dot{\overline{\varepsilon}}^p)}{\partial \overline{\sigma}_*}\Big|_T = kT\Psi_T \text{ where } \begin{cases} \Psi(\dot{\overline{\varepsilon}}^p)|_T & \text{for } \textbf{BCC} \\ \Psi(\overline{\varepsilon}^p, \dot{\overline{\varepsilon}}^p)|_T & \text{for } \textbf{FCC} \end{cases} \tag{2}$$

Here k is the Boltzmann constant and T the absolute temperature.

In addition, a common characteristic of many **FCC** metals is the appearance of a viscous drag component of flow stress at high rate of deformation [26,34,35]. For strain rate level varying as $10^3\,\text{s}^{-1} \leq \dot{\overline{\varepsilon}}^p \leq 10^4\,\text{s}^{-1}$ the flow stress sharply increases (Fig. 3).

Several explanations of this phenomenon have been proposed over the years. Many of them are based on a transition in the rate controlling deformation mechanism from thermal activation at low strain rates to some form of dislocation drag [37,38]. Some authors also account for strain rate history effects and relate this phenomenon to the strain rate sensitivity of structure evolution (*it makes the process intrinsically athermal*) [26,34]. According to Campbell and Ferguson [37] and Regazzoni et al. [39], when the viscous drag effect takes place, the equivalent stress may be defined as follows:

$$\overline{\sigma} = \overline{\sigma}_\mu + \overline{\sigma}^* + \overline{\sigma}_{vs} \tag{3 a}$$

$$\overline{\sigma}_{vs} \approx \kappa \dot{\overline{\varepsilon}}^p \tag{3 b}$$

where $\overline{\sigma}_{vs}$ is the viscous drag component (*independent of temperature* [17,40 42]) and κ is a material constant (*the viscous component is commonly assumed to be linearly dependent on strain rate* [37]). In the case of most **FCC** metals, the strain rate sensitivity cannot be defined using physical models based only on an Arrhénius type equation.

Taking into account the previous considerations, a constitutive relation for **FCC** metals with application to oxygen free high conductivity (OFHC) copper is developed. It is based on the original formulation proposed by Rusinek and Klepaczko (**RK**) [9]. The original **RK** formulation has a proven capacity for defining the
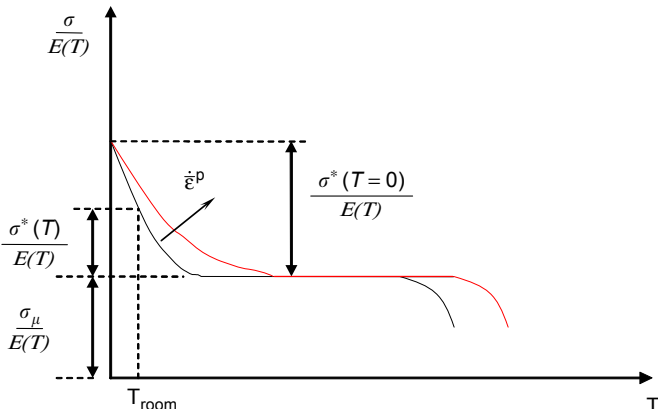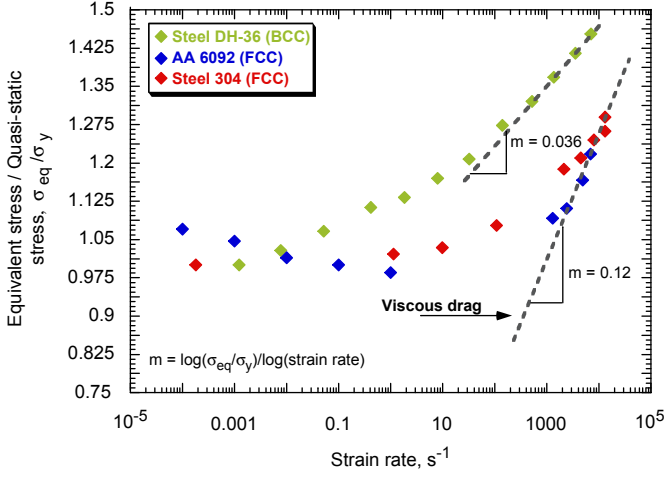
Fig. 3. Evolution of the normalized equivalent stress with strain rate for different **BCC** and **FCC** metals [10,34,36].

Fig. 4. Evolution of Young's modulus ratio with homologous temperature for different θ^* values.

thermo viscoplastic behaviour of many metallic alloys [28,43]. However, the **RK** model has to be modified in order to make it suitable for modeling determined **FCC** metals such as, for example, annealed OFHC copper.

In the following section of the paper the formulation of the modified **RK** model (**MRK**) proposed is reported.

3. An original constitutive model for FCC metals with application to OFHC copper

In the **MRK** constitutive relation the equivalent Huber Misses stress $\overline{\sigma}$ is decomposed in the following form:

$$\overline{\sigma} = \frac{E(T)}{E_0}[\overline{\sigma}_\mu + \overline{\sigma}^*] + \overline{\sigma}_{vs} \tag{4}$$

where each term here is defined as follows.

3.1. Temperature dependent Young's modulus $E(T)/E_0$

The factor $E(T)/E_0$ defines the Young's modulus evolution with temperature [44] as follows:

$$E(T) = E_0\left\{1 - \frac{T}{T_m}\exp\left[\theta^*\left(1 - \frac{T_m}{T}\right)\right]\right\}, T > 0 \tag{5}$$

where E_0, T_m and θ^* denote, respectively, the Young's modulus at $T = 0\,\mathrm{K}$, the melting temperature and the characteristic homo logous temperature. This expression allows definition of thermal softening depending on the crystal lattice [43] (Fig. 4). In the case of **FCC** metals $\theta^* \approx 0.9$ as reported by Rusinek et al. [43].

3.2. Internal stress component $\overline{\sigma}_\mu$

According to the considerations for **FCC** metals reported for example in [7,12,15,26] let us assume the athermal stress $\overline{\sigma}_\mu$ to be independent of plastic strain. As discussed previously, the yield stress in **FCC** metals may show reduced rate and temperature dependencies (*certain temperature effect is taken into account by the Young's modulus temperature dependence*). In agreement with [15] the athermal stress will be just tied to the initial yield stress
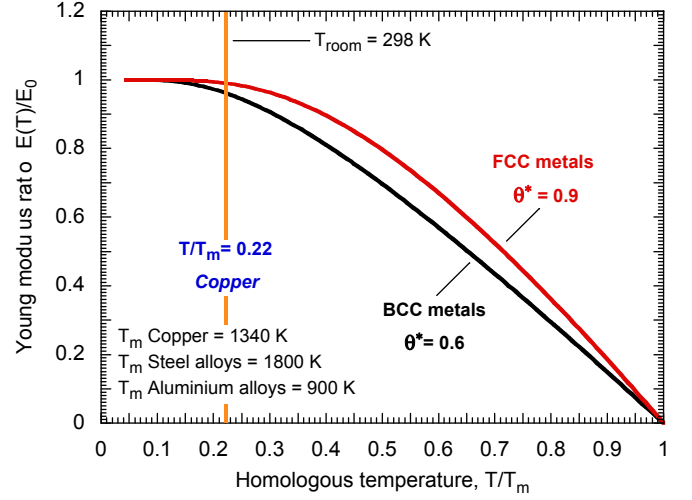
in the form

$$\overline{\sigma}_\mu = Y \tag{6}$$

where Y is the flow stress on undeformed material.

In comparison with the original formulation of the **RK** model, in the **MRK** formulation the athermal stress $\overline{\sigma}_\mu$ does not describe strain hardening of the material.

3.3. Effective stress component $\overline{\sigma}^*$

The effective stress $\overline{\sigma}^*$ is the flow stress component defining rate dependent interactions with short range obstacles. It denotes the rate controlling deformation mechanism from thermal activa tion. At temperatures greater than 0 K, thermal activation assists the applied stress. It reduces the stress level required to force dislocations past obstacles.

The theory of thermodynamics and kinetics of slip [6] is founded on a set of equations that relate activation energy ΔG, mechanical threshold stress (**MTS**) $\hat{\sigma}$, applied stress $\overline{\sigma}$, strain rate $\dot{\varepsilon}$, temperature T and determined physical material parameters. Based on such understanding of the material behaviour, Rusinek and Klepaczko [9] derived the following expression:

$$\overline{\sigma}^*(\overline{\varepsilon}^p, \dot{\overline{\varepsilon}}^p, T) = \sigma_0^*\left\langle 1 - \xi_1\left(\frac{T}{T_m}\right)\log\left(\frac{\dot{\varepsilon}_{max}}{\dot{\overline{\varepsilon}}^p}\right)\right\rangle^{1/\xi_2} \tag{7}$$

where ξ_1 and ξ_2 are material constants describing temperature and rate sensitivities of the material, respectively. T_m is the melting temperature and $\dot{\varepsilon}_{max}$ the maximum strain rate level for a particular material. This expression exhibits the relation between strain rate and temperature proven by many authors over the last decades [6,8 10].

As discussed previously, in many **FCC** metals the thermal activation processes have strain dependence. In agreement with the considerations reported in [7,12] such dependence may be formulated in the form

$$\sigma_0^* = \sigma_0^*(\overline{\varepsilon}^p) = B(\overline{\varepsilon}^p)^n \tag{8}$$

However, strain hardening is intrinsically dependent on strain rate and temperature. Based on the formulation reported in [9], a more suitable expression (*in comparison with* Eq. (8)) is proposed in the present paper as

$$\sigma_0^*(\overline{\varepsilon}^p, \dot{\overline{\varepsilon}}^p, T) = B(\dot{\overline{\varepsilon}}^p, T)(\overline{\varepsilon}^p)^{n(\dot{\overline{\varepsilon}}^p, T)} \tag{9}$$

3

Therefore, expression (8) becomes also rate and temperature dependent (Eq. (9)). Thus, the model considers dependences on strain and on strain rate that the mechanical threshold stress exhibits in the case of OFHC copper [26]. This definition is consistent with the dominance of dislocation obstacle interac tions in the plastic deformation of polycrystalline **FCC** materials [23,26]. In Eq. (9), the modulus of plasticity B defines rate and temperature sensitivities on strain hardening and n is the strain hardening exponent dependent on strain rate and temperature.

Explicit formulations describing the modulus of plasticity and the strain hardening exponent are given, respectively, as

$$B(\dot{\bar{\varepsilon}}^p, T) = B_0 \left(\left(\frac{T}{T_m} \right) \log \left(\frac{\dot{\varepsilon}_{max}}{\dot{\bar{\varepsilon}}^p} \right) \right)^{-v}, T > 0 \tag{10}$$

$$n(\dot{\bar{\varepsilon}}^p, T) = n_0 \left\langle 1 \quad D_2 \left(\frac{T}{T_m} \right) \log \frac{\dot{\bar{\varepsilon}}^p}{\dot{\varepsilon}_{min}} \right\rangle \tag{11}$$

where B_0 is a material constant, v is proportional to temperature sensitivity, n_0 is the strain hardening exponent at T = 0 K, D_2 is a material constant and $\dot{\varepsilon}_{min}$ is the lower limit of the model. The McCauley operator is defined as follows: $\langle \bullet \rangle = \bullet$ if $\langle \bullet \rangle \geq 0$ or $\langle \bullet \rangle = 0$ if $\langle \bullet \rangle \leq 0$.

3.4. Viscous drag component $\overline{\sigma}_{vs}$

The formulation used to define the viscous drag component $\sigma_{vs}(\dot{\bar{\varepsilon}}^p)$ was originally introduced in [40 42] and it has a semi physical character. It comes from the relation between viscous drag, strain rate and determined physical material parameters given as [40]

$$\overline{\sigma}_{vs} \approx \overline{\sigma}_{vs}(M, \rho_m, B, b, \dot{\bar{\varepsilon}}^p) \propto \dot{\bar{\varepsilon}}^p \tag{12}$$

where M is the Taylor factor, B the drag coefficient, ρ_m the mobile dislocation density and b the magnitude of the Burgers vector. The viscous drag component is proportional to the strain rate (Eq. (12)).

Thus, based on experimental observations, Kapoor and Nemat Nasser [40] set the following relations:

$$\overline{\sigma}_{vs}(\dot{\bar{\varepsilon}}^p) = \chi[1 \quad \exp(\quad \alpha)\dot{\bar{\varepsilon}}^p] \tag{13 a}$$

$$\alpha = \left(\frac{M^2 B}{\rho_m b^2 \tau_y} \right) \tag{13 b}$$

where χ is a material constant, α represents an effective damping coefficient affecting the dislocation motion and τ_y is the athermal yield stress [41,42]. Let us assume that $\tau_y = Y$ as described before in Eq. (6). In comparison with the original **RK** formulation, this expression for $\overline{\sigma}_{vs}$ (Eqs. (13 a, 13 b)) allows the **MRK** model to describe the rate sensitivity of **FCC** metals under fast loading.

In the case of adiabatic conditions of deformation the constitutive relation is combined with the energy balance principle in Eq. (14). This relation allows for an approximation of the thermal softening of the material by adiabatic heating.

$$\Delta T(\overline{\varepsilon}^p, \overline{\sigma}) = \frac{\beta}{\rho C_p} \int_0^{\overline{\varepsilon}_{max}^p} \overline{\sigma}(\overline{\varepsilon}^p, \dot{\overline{\varepsilon}}^p, T) d\overline{\varepsilon}^p \tag{14}$$

where β is the Taylor Quinney coefficient assumed as constant (interesting considerations concerning the potential dependence of Taylor Quinney coefficient on plastic deformation are reported in [45,46]), ρ the material density and C_p the specific heat at constant pressure. Transition from isothermal to adiabatic condi tions is assumed at $\dot{\bar{\varepsilon}}^p = 10 \, \text{s}^{-1}$ in agreement with experimental observations and numerical estimations reported for example in [29,47].

Finally, some comments have to be made concerning the definition of the strain rate sensitivity provided by the **MRK** constitutive relation.

The model takes into account only the instantaneous rate sensitivity of the material. Instantaneous strain rate sensitivity describes the rate dependent behaviour of metals during con tinuous loading condition (*current value of flow stress is an instantaneous function of strain ε^p, strain rate $\dot{\varepsilon}^p = 10 \, \text{s}^{-1}$ and temperature T*) [48]. Many of the constitutive descriptions reported in the literature (*physical based models as well as phenomenological models*) [1,3 5,7 10] are usually restricted to such application fields.

However, it is known that strain rate history effects are present in the material deformation behaviour. As described by [49 51] historical effects may be of relevance for modeling the material behaviour when it is subjected to an abrupt increase of applied deformation rate or to a cycling loading process.

In order to take into account such considerations, definitions of internal state variables in the formulation of the constitutive description are necessary [11,14]. Such internal state variables are traditionally chosen as the evolution of dislocation density [52] or, in a wider sense, as an effective microstructural length governed by a determined evolution law [11,14].

Such potential improvements of the **MRK** model (*definitions of internal state variables are not considered in the present formulation*) may be approached in forthcoming works in order to extend its validity to, for example, a proper description of cycling loading processes. However, it must be pointed out this will lead to a more complex formulation, increasing the difficulty for its implementa tion into **FE** codes and augmenting its computational time. Therefore, it may reduce the suitability of the **MRK** constitutive relation to engineering applications such as perforation or HSM, which require discretization models involving a large number of degrees of freedom.

Subsequently, a straightforward method for model calibration is reported. This allows the model parameters to be defined step by step. Contrary to other constitutive descriptions, the procedure does not involve a global fitting.

4. A systematic procedure for the calculation of model parameters

The main steps necessary for defining the model parameters are as follows:

i. The athermal component of the flow stress, Y, is estimated as the flow stress on undeformed material [26].

ii. Subsequently, the flow stress level along with temperature for different plastic strain levels under quasi static loading is plotted [15] (Fig. 5a). For each plastic strain level, let us assume, as a first approximation, that the experimental data follow a linear trend [15] (Fig. 5a). The intersection of the fitting curves with $T = 0 \, \text{K}$ (**MTS** *evolution with increasing deformation*) are represented along with plastic deformation. These points are fitted with Eq. (9) (Fig. 5b). A first estimation for B and n is obtained.

iii. For **FCC** metals, the strain rate sensitivity within the range only controlled by thermally activated deformation mechan isms may be approximated by a function of the type $\overline{\sigma} \propto \log(\dot{\bar{\varepsilon}}^p)$ [34,37 39]. Such a rate sensitivity drastically changes when viscous drag deformation mechanisms take place. In this case the relation $\overline{\sigma} \propto \dot{\bar{\varepsilon}}^p$ is fulfilled as reported previously. The strain rate level defining the appearance of deformation mechanisms due to viscous drag, $\dot{\bar{\varepsilon}}^p_{drag}$, has to be
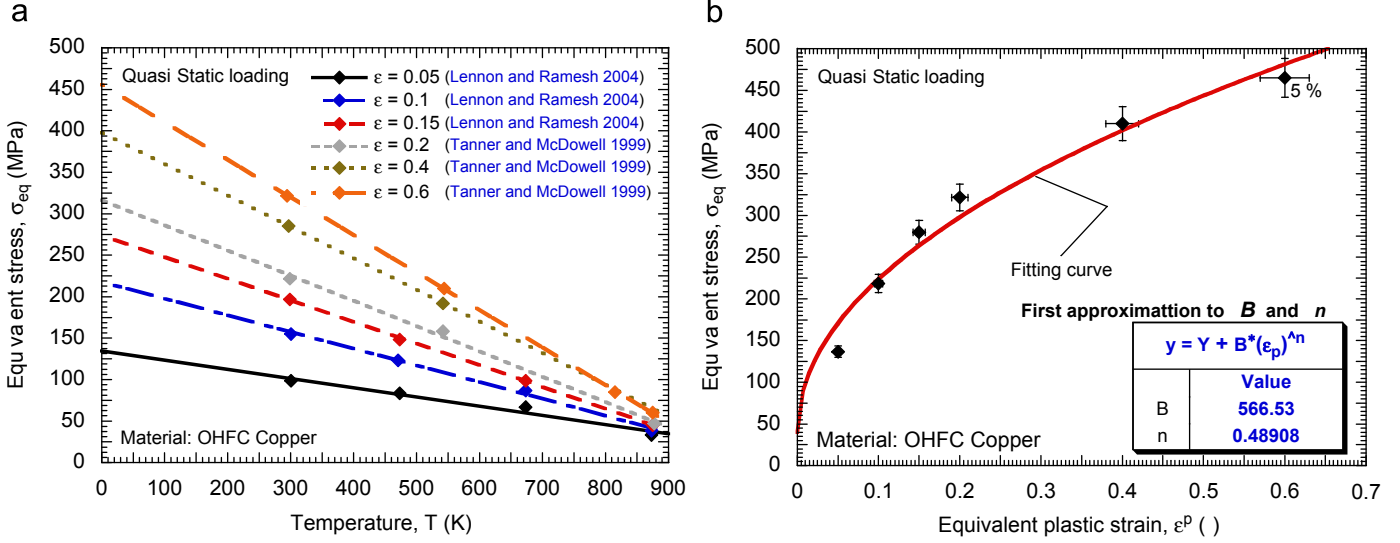
Fig. 5. (a) Evolution of the flow stress with temperature for different deformation levels [23,53] and fitting following a linear trend. (b) Flow stress evolution at $T \approx 0$ K (**MTS**) with plastic deformation, and fitting using the hardening function.

identified from experiments. In the range $\dot{\bar{\varepsilon}}^p \leq \dot{\bar{\varepsilon}}^p_{drag}$ the stress increase is defined as follows:

$$\Delta\overline{\sigma}(\dot{\bar{\varepsilon}}^p_{reference} \rightarrow \dot{\bar{\varepsilon}}^p)|_{\overline{\varepsilon}^p} = \overline{\sigma}(\dot{\bar{\varepsilon}}^p)|_{\overline{\varepsilon}^p} \quad \overline{\sigma}(\dot{\bar{\varepsilon}}^p_{reference})|_{\overline{\varepsilon}^p} = \overline{\sigma}^*(\dot{\bar{\varepsilon}}^p,T)|_{\overline{\varepsilon}^p} \quad (15)$$

Combining Eq. (15) with experimental results for an imposed strain level $\overline{\varepsilon}^p$, it is possible to determine the material constants ξ_1 and ξ_2. The strain level should be assumed as $\overline{\varepsilon}^p \leq 0.1$ in order to guarantee the isothermal condition of deformation. For larger strain values, the adiabatic condition induces a thermal softening of the material and a decrease in strain hardening.

iv. In the case $\dot{\bar{\varepsilon}}^p_{drag} \leq \dot{\bar{\varepsilon}}^p$ the stress difference between the model predictions (*without viscous drag component*) and experiments is due to the viscous drag term $\overline{\sigma}_{vs}(\dot{\bar{\varepsilon}}^p)$ (Fig. 6). By combination of Eq. (13 a) with experimental results for an imposed strain level $\overline{\varepsilon}^p$, it is possible to determine the material constants χ and α (Fig. 6).

v. The last step is the application of Eq. (4), combined with experimental results $\overline{\sigma} \quad \overline{\varepsilon}^p|_{\dot{\bar{\varepsilon}}^p}$. Then, the stress dependency on temperature and strain rate for the modulus of plasticity B and the strain hardening exponent n can be defined.

5. Application and validation of the constitutive relation for modeling the thermo-viscoplastic behaviour of OFHC copper

Using the procedure reported in the previous section, the model has been calibrated for annealed OFHC copper using the experimental data collected from [8,23,34,53]. The set of constants found is presented in Tables 1 and 2. Conventional physical constants of OFHC copper can be obtained from material handbooks (Table 3).

Copper is a ductile metal with very high thermal and electrical conductivity. Such properties make it attractive in electrical applications, piping, manufacture of semiconductors and super conductor components. It also finds application for shaped charge liners. This part of shaped charges is for forming a jet that penetrates targets [54,55]. Liner material is required to be of excellent ductility and high density. Shaped charges are frequently used for military applications, although the most extensive use
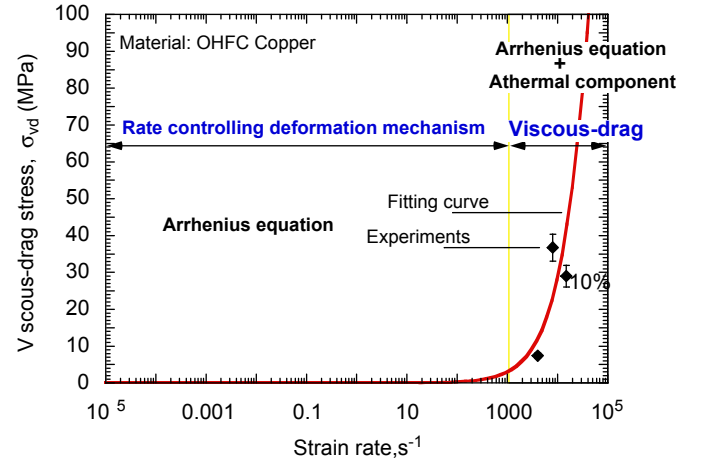

Fig. 6. Calibration of the viscous drag stress component for OFHC annealed copper using experimental data reported in [8].

today of shaped charges is in the oil and gas industry to pierce metal, concrete and other solid materials [54,55]. Next, predictions of the **MRK** model are compared with experiments.

The first step is to evaluate predictions of the **MRK** model for different strain rate levels at room temperature. In Fig. 7 a satisfactory agreement between model and experiments is reported under quasi static loading $\dot{\bar{\varepsilon}}^p = 0.001\,\text{s}^{-1}$ (Fig. 7a) as well as under dynamic loading $\dot{\bar{\varepsilon}}^p = 4000\,\text{s}^{-1}$ (Fig. 7b). It must be pointed out that the analytical predictions fit properly not only the flow stress level but also the strain hardening of the material up to a plastic strain level close to $\overline{\varepsilon}^p \approx 1$. Only in the case of high strain rate and large deformation $\overline{\varepsilon}^p > 0.75$, Fig. 7b, the material reaches saturation stress condition and differences between experiments and model predictions appear.

Such an agreement with experiments extends within the strain rate variation range of $10^{-4}\,\text{s}^{-1} \leq \dot{\bar{\varepsilon}}^p \leq 10^4\,\text{s}^{-1}$ as shown in Fig. 8. The viscous drag component has great relevance on the description of material behaviour when subjected to high rate of deformation. It compensates the underestimation on flow stress at high strain rate that would be obtained using only an Arrhenius type equation as a mechanism to describe the rate sensitivity of the material (Fig. 8).

Table 1
Constants determined for annealed OFHC copper for thermal and athermal stress components of the **MRK** model.

Y (MPa)	B_0 (MPa)	v (−)	n_0 (−)	D_2 (−)	ξ_2 (−)	ξ_1 (-)	T_m (K)	$\dot{\varepsilon}_{min}$ (s⁻¹)	$\dot{\varepsilon}_{max}$ (s⁻¹)	θ^* (−)
40	560.28	0.30447	0.492	0.0553	0.0131	0.0011932	1340	10^{-5}	10^7	0.9

Table 2
Constants determined for annealed OFHC Copper for the viscous drag stress component of the **MRK** model.

χ (MPa)	α (−)
249	0.0000122

Table 3
Physical constants for annealed OFHC copper.

E_0 (GPa)	C_p (J kg K⁻¹)	β (−)	ρ (kg m⁻³)
130	385	0.9	8960

In Fig. 9 the experimental data are compared with analytical predictions of the model for two different initial temperatures at a high strain rate $\dot{\bar{\varepsilon}}^p = 4000\,\text{s}^{-1}$. In both cases the model defines correctly strain hardening and flow stress level of the material.

Moreover, the temperature sensitivity of the material is well defined in the range $100\,\text{K} \leq T \leq 1100\,\text{K}$ as shown in Fig. 10. It must be noticed that within this range of initial temperatures the flow stress of the material is continuously decreasing. A temperature independent region is not observed. This behaviour is in agreement with considerations reported for example by Voyiadjis and Almasri [15] for annealed OFHC copper.

In the following section of this paper the analytical predictions of **MRK** model are compared with those obtained from physical based models reported in the international literature.

6. Comparison of constitutive relations with applications to OFHC copper

The constitutive relations are those due to Nemat-Nasser and Li (**NNL**) [8] and due to Voyiadjis and Almasri (**VA**) [15], both of which are introduced.

6.1. Formulation of the Nemat-Nasser–Li constitutive relation

According to the considerations reported for example in [7,24,25], the **NNL** constitutive relation (*like the* **MRK** *model*) decomposes the equivalent Huber–Misses stress $\overline{\sigma}$ into thermal $\overline{\sigma}^*(\overline{\varepsilon}^p, \dot{\overline{\varepsilon}}^p, T)$ and athermal $\overline{\sigma}_\mu(\overline{\varepsilon}^p)$ components:

$$\overline{\sigma}(\overline{\varepsilon}^p, \dot{\overline{\varepsilon}}^p, T) = \overline{\sigma}_\mu(\overline{\varepsilon}^p) + \overline{\sigma}^*(\overline{\varepsilon}^p, \dot{\overline{\varepsilon}}^p, T) \tag{16}$$

The athermal stress term, which defines hardening of material, is a function only of plastic strain:

$$\overline{\sigma}_\mu(\overline{\varepsilon}^p) = \sigma_a^0 (\overline{\varepsilon}^p)^{n_1} \tag{17}$$

where σ_a^0 and n are material constants describing the flow stress level and the strain hardening of the material respectively.

On the other hand, the thermal stress is defined by Eq. (18). It depends not only on strain rate and temperature but also on plastic deformation. As previously discussed, such dependence is in agreement with the considerations reported in [7,8,12,23] for determined **FCC** metals like OFHC copper.

$$\overline{\sigma}^*(\overline{\varepsilon}^p, \dot{\overline{\varepsilon}}^p, T)$$

$$= \sigma^0 \left(1 - \left(-\frac{kT}{G_0} \left(\ln\left(\frac{\dot{\overline{\varepsilon}}^p}{\dot{\overline{\varepsilon}}_0}\right) + \ln(1 + a(T)(\overline{\varepsilon}^p)^{n_0}) \right) \right)^{1/q} \right)^{1/p}$$
$$\times (1 + a(T)(\overline{\varepsilon}^p)^{n_0}) \tag{18}$$

where σ^0 is a material constant, k is the Boltzmann constant, G_0 the reference Gibbs free energy at $T = 0\,\text{K}$ (*it can be considered as an empirical parameter* [8]), $\dot{\varepsilon}_0$ the reference strain rate, n_0 is a material constant defining strain hardening, and p and q are parameters describing the profile of the short range energy barrier to the motion of dislocations.

Moreover, $a(T)$ is an empirical function depending on temperature and tied to the average dislocation spacing (Eq. (19)). It contributes to the definition of the strain hardening of the material.

$$a(T) = a_0 \left(1 - \left(\frac{T}{T_m}\right)^{n_2} \right) \tag{19}$$

where a_0 and n_2 are material constants.

Some comments must be made concerning this constitutive relation. They are outlined below.

- Strain hardening is defined without taking into account the intrinsic effect of strain rate. The constancy of the strain hardening exponents n_i in the formulation is contrary to observations frequently made and reported for metals in many publications, for example [28,29,51]. This fact may raise considerable relevance, especially in dynamic events susceptible for plastic instabilities [18,28,56].
- The model in its present form does not include the definition of electron and phonon drag effects (*viscous drag influence*), which may be of relevance at high strain rates and temperatures. However, in recent works [40–42] Nemat-Nasser and co-workers gather such information for modeling **FCC** materials.
- The constitutive relation does not account for the dependence of Young's modulus with temperature. It may lead to under estimation of the temperature sensitivity of the material.

More details concerning the formulation of the model and the calibration procedure can be found in [8]. The material constants reported for annealed OFHC copper are presented in Table 4 [8].

It must be pointed out that using the previous calibration, **NNL** model defines an athermal region in the material behaviour, which is shown in Fig. 11a. Such an analysis was conducted by calculating the combination of deformation rate and temperature, which, for an imposed plastic strain, satisfies the condition $\overline{\sigma}^* = 0$ (Eq. (18)). Thus, for determined loading conditions the flow stress of the material is not affected by temperature increase (Fig. 11). This behaviour is different from that predicted by the **MRK** model, Fig. 11b, and may not be in agreement with experiments reported for annealed OFHC copper. This consideration will be analyzed more exhaustively later in the present paper.

6.2. Formulation of the Voyiadjis–Almasri constitutive relation

Voyiadjis and Almasri [15] derived a physically based model founded on the concept of thermal activation analysis. As for the previous constitutive descriptions introduced in this paper, the
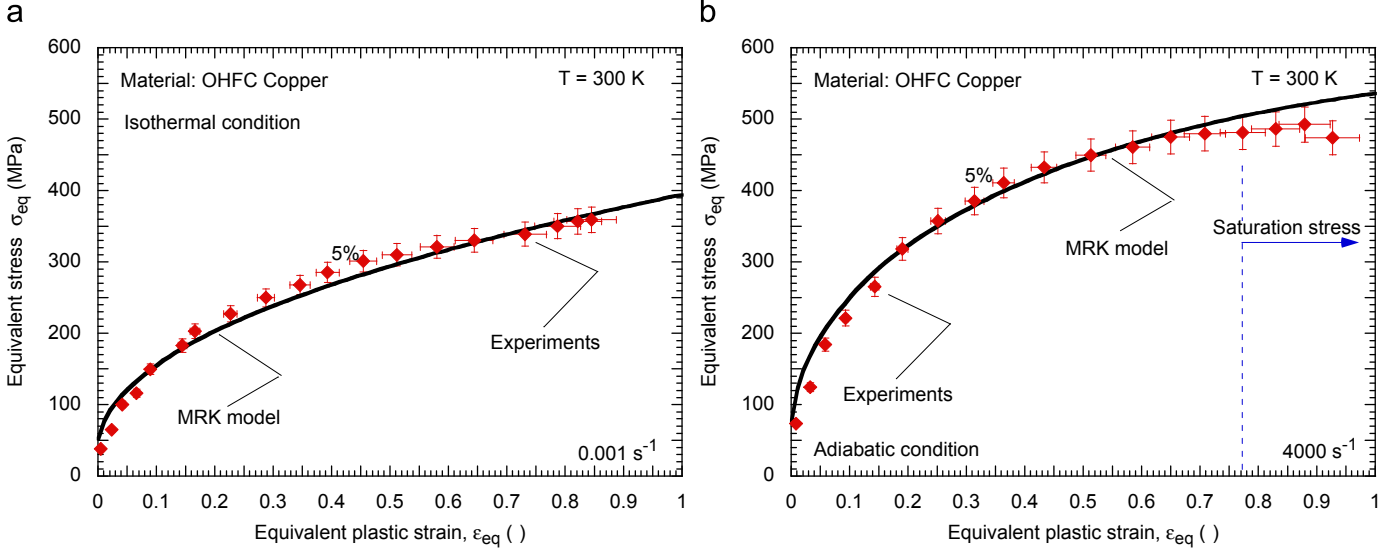
Fig. 7. Description of the flow stress evolution along plastic strain using **MRK** model and comparison with experiments at room temperature [8]: (a) 0.001 and (b) 4000 s $^{-1}$.
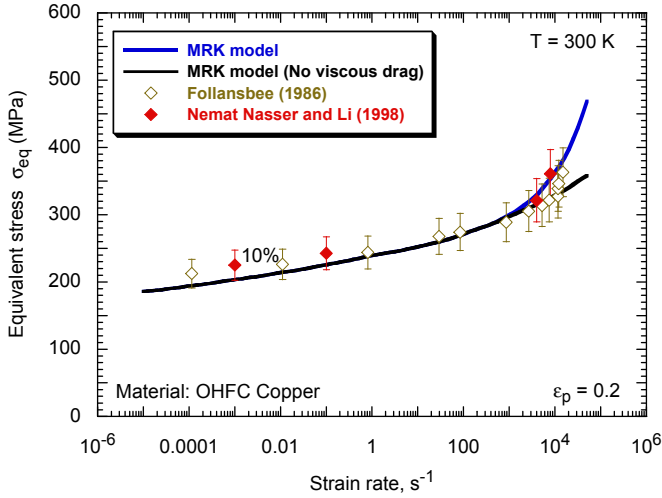

Fig. 8. Description of the flow stress evolution with strain rate using the **MRK** model and comparison with experiments at room temperature, $\bar{\varepsilon}^p$ 0.2 [8,34].

equivalent Huber Misses stress $\overline{\sigma}$ is split into two parts, the equivalent thermal stress $\overline{\sigma}_\mu$ and the equivalent athermal stress $\overline{\sigma}^*(\overline{\varepsilon}^p, \dot{\overline{\varepsilon}}^p, T)$:

$$\overline{\sigma}(\overline{\varepsilon}^p, \dot{\overline{\varepsilon}}^p, T) = \overline{\sigma}_\mu + \overline{\sigma}^*(\overline{\varepsilon}^p, \dot{\overline{\varepsilon}}^p, T) \tag{20}$$

The athermal stress is defined without dependence on plastic strain, which corresponds to ideal plasticity:

$$\overline{\sigma}_\mu = Y_a \tag{21}$$

where Y_a is a material constant describing the stress component independent of temperature and strain rate.

The thermal stress is defined as a function of plastic strain (Eq. (22)). It is derived from the concept of dislocation kinetics [6].

$$\overline{\sigma}^*(\overline{\varepsilon}^p, \dot{\overline{\varepsilon}}^p, T) = (B\overline{\varepsilon}_p^n)\left(1 + B_1 T(\dot{\overline{\varepsilon}}_p)^{1/m} \quad B_2 T \exp\left(A\left(1 \quad \frac{T}{T_t}\right)\right)\right) \tag{22}$$

Here B denotes the modulus of strain hardening, n is the strain hardening exponent, B_1 and B_2 are material constants tied,

basically, to mobile dislocation density evolution and to thermo dynamic material parameters [15], m defines the strain rate sensitivity and A is a material constant.

Some comments must be made concerning this constitutive relation. They are outlined below.

- As reported for the **NNL** model, in the **VA** constitutive description, strain hardening is defined without taking into account the intrinsic effect of strain rate.
- The expression used to define the velocity of dislocations [57] leads to a formulation of the rate sensitivity of the form $\Delta\sigma(\dot{\overline{\varepsilon}}_i^p \to \dot{\overline{\varepsilon}}_{i+1}^p)|_{\overline{\varepsilon}_p}^T \propto (\dot{\overline{\varepsilon}}^p)^{1/m}$. This expression neglects rate sensitivity under quasi static loading, overestimating it under dynamic loading (Fig. 12).
- Temperature and rate sensitivities are decoupled in the formulation of the model. From the thermal activation analysis, and based on an Arrhénius type equation, many researchers reported the existence of reciprocity between strain rate and temperature [6,25,58].
- As reported for the **NNL** model, the **VA** constitutive relation does not account for the dependence of Young's modulus with temperature.

More details concerning the formulation of the model and the calibration procedure can be found in [15]. The material constants reported for annealed OFHC copper are listed in Table 5 [15].

Next, analytical predictions of **MRK**, **NNL** and **VA** constitutive relations are compared and collated with experimental data reported in [8,34].

6.3. Analysis and comparison of constitutive relations

In Fig. 13 the analytical predictions of the three models described previously (**MRK, NNL and VA models**) and their comparisons with experiments for two different strain rate levels at room temperature are depicted. Under quasi static loading, Fig. 13a, all models offer predictions in agreement with experiments. Flow stress level and strain hardening are well described. The maximum disagreement is reached for **NNL** model at large deformation. Under high loading rate, Fig. 13b, the predictions obtained from the **MRK** model offer a better fitting
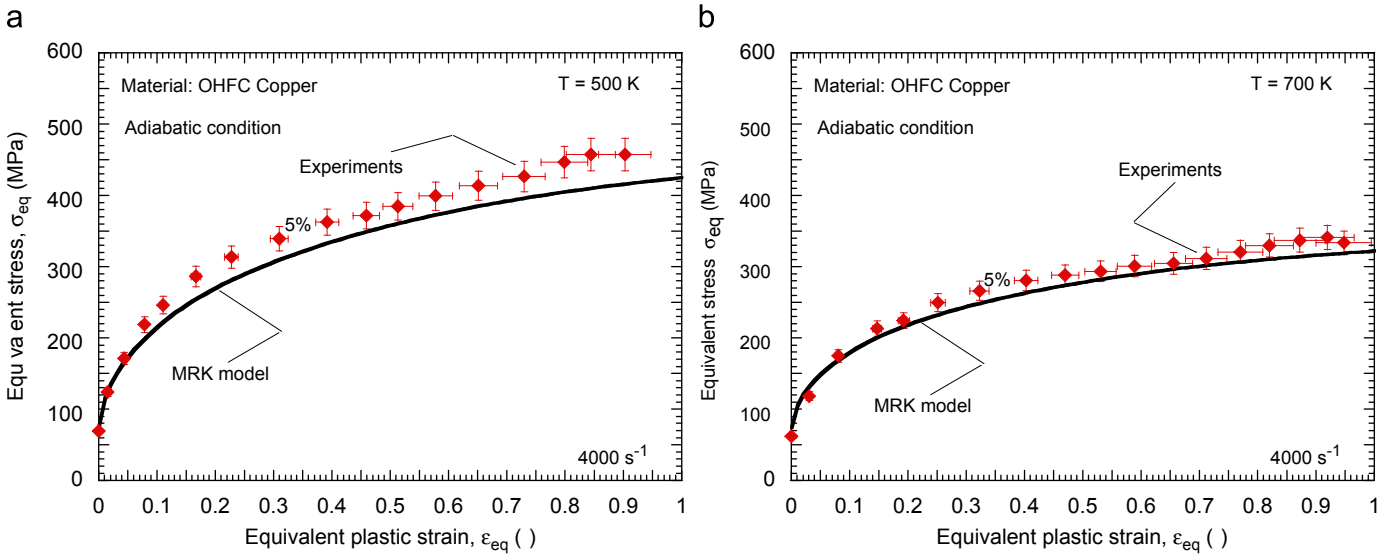
Fig. 9. Description of the flow stress evolution with plastic strain using the **MRK** model and comparison with experiments at 4000 s^{-1} [8]. (a) T_0 = 500 K and (b) T_0 = 700 K.
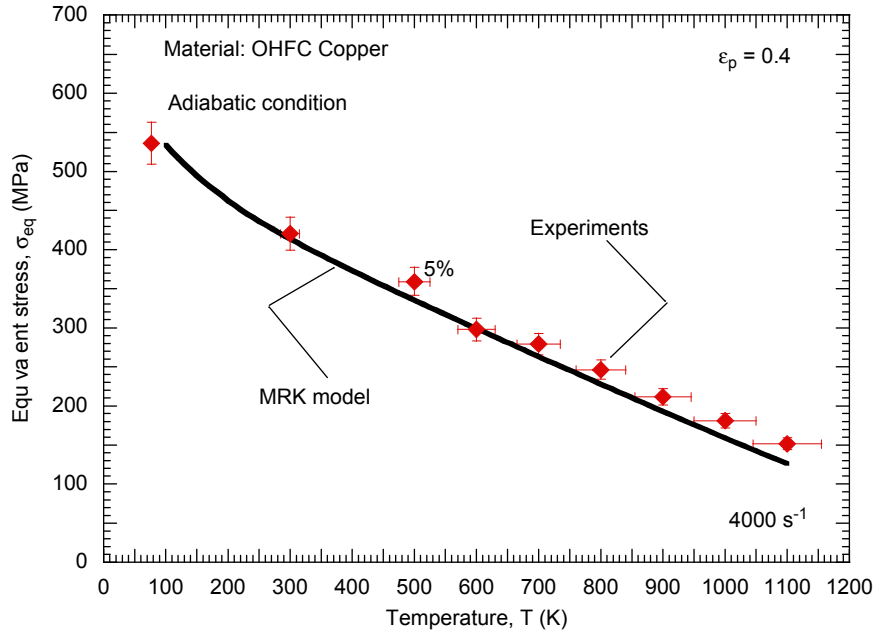

Fig. 10. Description of the flow stress evolution with temperature using the **MRK** model and comparison with experiments at 4000 s^{-1} and ε^p = 0.4 [8].

Table 4
Constants determined for annealed OFHC copper for the **NNL** model [8].

p (–)	q (–)	k/G_0 (K^{-1})	ε_0 (s^{-1})	a_0 (–)	σ^0 (MPa)	σ_a^0 (MPa)	n_0 (–)	n_1 (–)	n_2 (–)
2/3	2	0.000049	2×10^{10}	20	46	220	0.5	0.3	2

with the experimental data in comparison with other constitutive descriptions. In this case, although **NNL** and **VA** relations describe properly the strain hardening evolution, they underestimate the flow stress level (Fig. 13b).

In order to evaluate the description of rate sensitivity proposed by each model, their definition of the flow stress evolution along with strain rate is shown in Fig. 14. Two different plastic strain values are considered, $\bar{\varepsilon}_p = 0.1$ (Fig. 14a) and $\bar{\varepsilon}_p = 0.15$ (Fig. 14b).

In comparison with the predictions provided by the **MRK** model, **NNL** defines a slightly larger value of stress until a certain strain rate level is reached. Beyond this point, the **NNL** model underestimates flow stress of the material since it does not account for the dislocation drag effect, which takes place at high strain rates in annealed OFHC copper. Moreover, the **VA** model does not define properly the rate sensitivity of the material. As commented on before, the **VA** constitutive relation neglects rate sensitivity up to the high strain rate level achieved, $\dot{\bar{\varepsilon}}_p \approx 1000 \, \text{s}^{-1}$ (Fig. 14). In the case of $\dot{\bar{\varepsilon}}_p \geq 1000 \, \text{s}^{-1}$, the rate sensitivity proposed is excessive (Fig. 14).

As previously introduced, the description of rate sensitivity is related to **VTA**. Using Eq. (2) it is possible to analyze for each model the evolution of **VTA** along with deformation rate for different plastic strain levels (Fig. 15). Although the models considered define a typical decrease of **VTA** with plastic strain
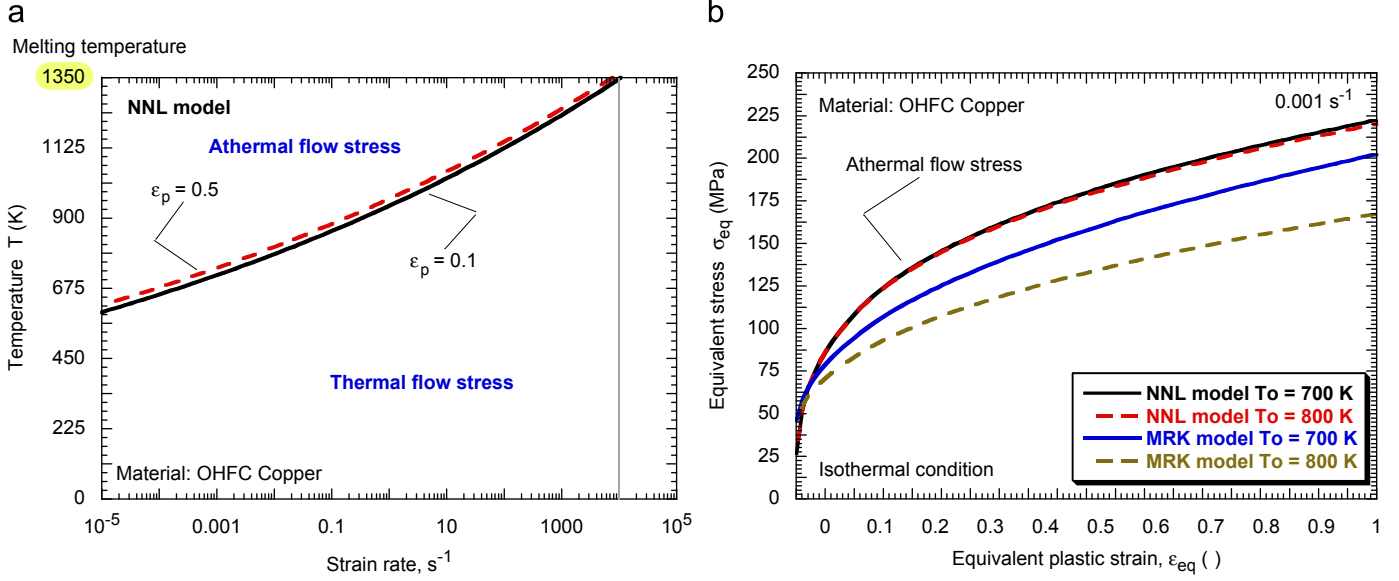
Fig. 11. (a) Definition of thermal and athermal regions predicted by the model along with temperature and strain rate for different plastic strain levels. (b) Evolution of flow stress with deformation for the **NNL** and **MRK** models at $T_0 = 700\,\text{K}$ and $T_0 = 800\,\text{K}$ under quasi-static loading.
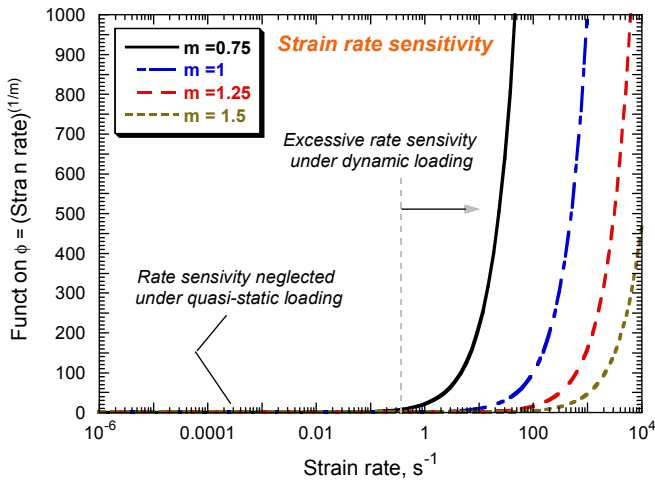

Fig. 12. Evolution of the function $\phi = (\dot{\bar{\varepsilon}}_p)^{1/m}$ with increasing strain rate.

Table 5
Constants determined for annealed OFHC copper for the **VA** model [15].

Y_a (MPa)	B_0 (MPa)	n (−)	B_1 (−)	B_2 (−)	m (−)	A (−)	T_t (K)
0	600	0.42	0.0000004	0.001	1.15	0.001	610

taking place in many **FCC** metals [7,15,32] (Fig. 15), considerable differences among the predictions are observed (Fig. 15).

In comparison with the **MRK** relation, the **NNL** model exhibits larger values of **VTA** within the range $\dot{\bar{\varepsilon}}_p \geq 10^{-3}\,\text{s}^{-1}$. This means a lower contribution of the thermal component to the overall flow stress (*it has been analyzed more exhaustively ahead in the present paper*). Due to the low rate sensitivity proposed by the **NML** relation, the slope of the curves $\Psi - \log(\dot{\bar{\varepsilon}})$ is smaller than in the case of the **MRK** model (Fig. 15). For the **MRK** model as the loading rate increases, **VTA** quickly decreases. This behaviour is in

agreement with considerations reported for example in [30]. As thermal activation reduces its effect on assisting dislocations to overcome obstacles, flow stress of the material increases. Moreover, it must be pointed out that, in the **NNL** and **MRK** models, thermal activation is present for the whole range of strain rates considered (*at room temperature*). **VTA** does not reach zero although viscous drag effects may take place (*they do not have to be taken into consideration for thermal activation analysis*; Fig. 15).

The description of **VTA** proposed by the **VA** model is quite different from those reported for the **NNL** and **MRK** models. The **VA** constitutive relation defines **VTA** only within the small range $10^2\,\text{s}^{-1} \leq \dot{\bar{\varepsilon}}_p \leq 10^3\,\text{s}^{-1}$ (Fig. 15). In the case of $\dot{\bar{\varepsilon}}_p \leq 10^2\,\text{s}^{-1}$ it shows a vertical asymptote (Fig. 15). This behaviour is a consequence of neglecting the rate sensitivity of the material for $\dot{\bar{\varepsilon}}_p \leq 10^2\,\text{s}^{-1}$ and is not in agreement with considerations reported for example in [30]. In the case of $10^3\,\text{s}^{-1} \leq \dot{\bar{\varepsilon}}_p$ the **VTA** reaches zero (Fig. 15). This consideration also is not in agreement with observations reported for example in [30].

Next, predictions of the models and their comparison with experiments are shown for different initial temperatures at a high strain rate level $\dot{\bar{\varepsilon}}_p \approx 4000\,\text{s}^{-1}$ (Fig. 16). At low temperature $T = 77\,\text{K}$, the **VA** model shows a great underestimation of the flow stress (Fig. 16a). On the contrary, **MRK** and **NNL** relations predict correctly the flow stress level and the strain hardening of the material from undeformed condition up to $\bar{\varepsilon}_p \approx 1$. For these constitutive relations (**MRK** and **NNL**) the difference with experiments takes place only at the beginning of loading. For a larger value of initial temperature, $T = 600\,\text{K}$, Fig. 16b, the three constitutive relations exhibit predictions in agreement with experiments. However, as the temperature increases, Figs. 16c and d, the **VA** model starts to overestimate the flow stress.

The temperature sensitivity proposed by each model can be well observed in the following curves (Fig. 17). The **VA** relation shows temperature sensitivity lower than that observed in experiments. At low temperature it clearly underestimates the flow stress, and at high temperatures it clearly overestimates it. Moreover **MRK** and **NNL** relations exhibit similar analytical predictions, close to experiments for the cases considered.
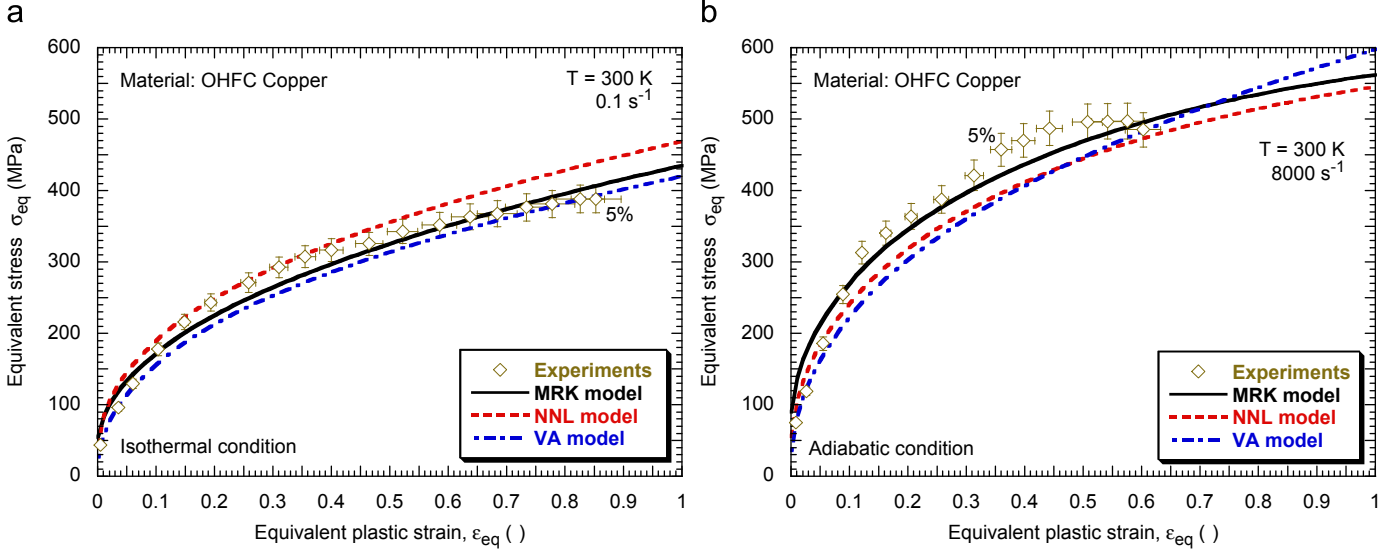
Fig. 13. Description of the flow stress evolution with plastic strain using the **MRK**, **NNL** and **VA** models and comparison with experiments at room temperature: (a) 0.1 and (b) 8000 s^{-1}[8].
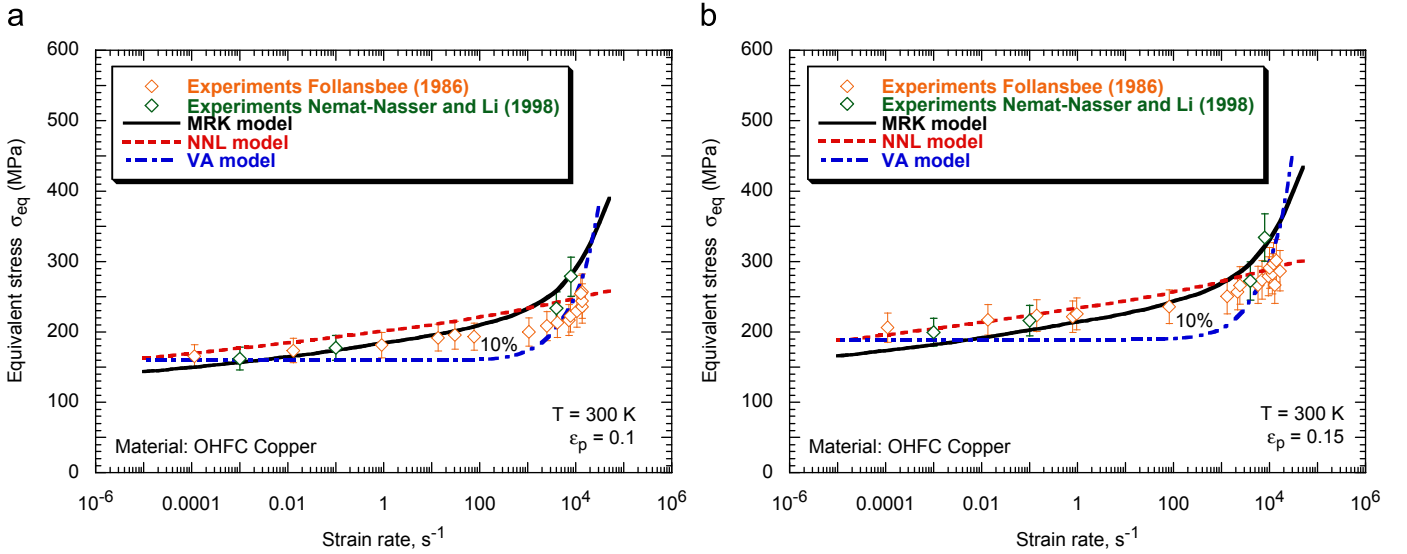

Fig. 14. Description of the flow stress evolution with strain rate using the **MRK**, **NNL** and **VA** models and comparison with experiments at room temperature: (a) ε^p 0.1 and (b) ε^p 0.15 [8,34].

However, differences between these two models appear at high temperature, $T_0 \geq 700$ K. Beyond this temperature level, the **MRK** model predicts uniformly decreasing flow stress ($d\overline{\sigma}_{eq}/dT \approx cte$) while the **NNL** model predicts a decrease in temperature sensitivity ($d\overline{\sigma}_{eq}/dT|_{T_0 \leq 700K} \geq d\overline{\sigma}_{eq}/dT|_{T_0 > 700K}$; Fig. 17).

This behaviour is caused by the definition of the effective stress proposed by each model. In Fig. 18 the evolution of the effective stress with increasing temperature for different deformation levels and different strain rate values is depicted. First, it must be noticed that in agreement with theoretical considerations reported in [7,8,12,23] for annealed OFHC copper, the thermal stress increases with plastic deformation (Fig. 18).

Moreover, differences in the level of the thermal stress are observed depending on the constitutive relation (Fig. 18). The effective stress level proposed by the **NNL** model is always lower than that corresponding to the **MRK** model (Fig. 18). The **NNL** model predicts athermal flow stress beyond a determined

temperature level (*which depends on the deformation rate*; Fig. 18). This means that under certain loading conditions annealed OFHC copper does not exhibit influence of temperature on flow stress. This behaviour may not be in agreement with experimental observations reported for this material (*previously showed in the present paper*; Fig. 5). Moreover, the effective stress of **MRK** model never reaches zero (Fig. 18). This model predicts absence of athermal region for annealed OFHC copper in agreement with [15].

7. Concluding remarks

In this paper a constitutive relation suitable for defining the thermo viscoplastic behaviour of **FCC** metals with dependence of strain on thermal activation is presented. The model is founded on physical aspects of the material behaviour. The proposed
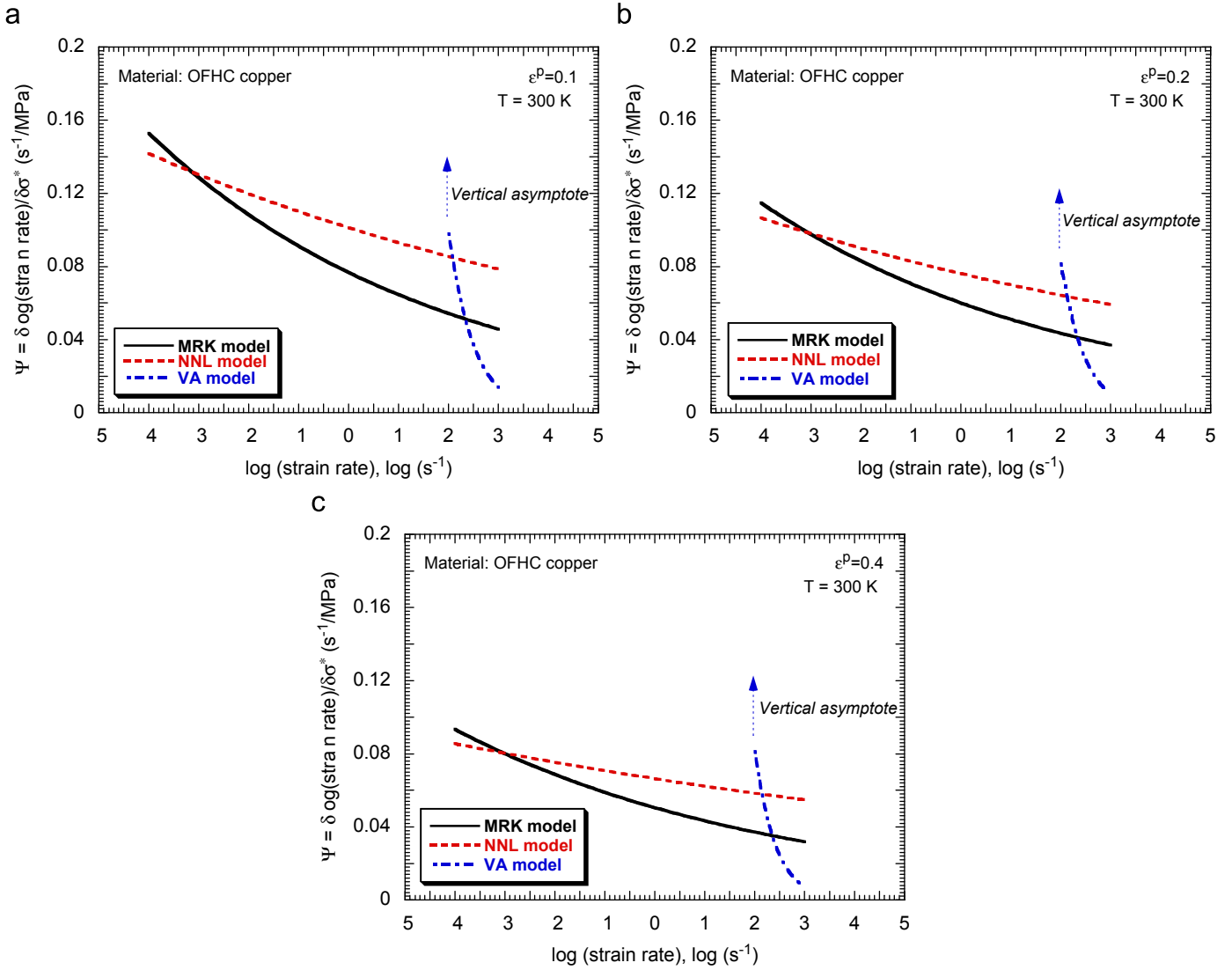
10

Fig. 15. Evolution of ψ with log(strain rate) using the **MRK**, **NNL** and **VA** models at room temperature: (a) ε^p 0.1, (b) ε^p 0.2 and (c) ε^p 0.4.

constitutive description has simplicity of formulation and easy calibration. It has been calibrated and used to study the behaviour of annealed OFHC copper. Its analytical predictions are compared with those obtained from other physically based models reported in the literature, namely those due to Voyiadjis and Almasri [15] and Nemat Nasser and Li [8]. From the analysis conducted the following conclusions can be reached:

- Determined **FCC** metals like OFHC copper exhibit dependence of strain on thermal activation. In such materials Peierls stress is relatively unimportant; the rate controlling deformation mechanism is used to overcome dislocation forests by individual dislocations. Strain hardening tends to be highly temperature and strain rate dependent, while the yield stress may show reduced dependence to such effects. These physical considerations are exhibited in the formulation of the model proposed.
- Taking account of viscous drag effects is a key factor in order to describe properly the rate and temperature sensitivities of the material under high rate loading. In addition, this provides extended flexibility to the model proposed. The strain rate

sensitivity of many **FCC** metals cannot be defined using only the rate temperature reciprocity proposed by an Arrhénius type equation.
- Predictions provided by the **MRK** model get satisfactory agreement with the experimental data taken as reference. This agreement is comparable to that obtained using **NNL** and **VA** models for the whole range of strain rates and initial temperatures considered.
- From the analysis of the thermal activation behaviour proposed by each formulation, the main importance of taking into account the rate temperature reciprocity in order to describe the material behaviour is revealed. This consideration places the **MRK** and **NNL** models in certain advantage in comparison with the **VA** model for describing the deformation behaviour of annealed OFHC copper.

The **MRK** model is revealed as a good alternative to other physically based relations proposed in the literature for modeling behaviour of determined **FCC** metals. Combination of physical background with a limited number of material constants makes it attractive for applications, where a proper definition of rate and temperature sensitivities of the material is required.
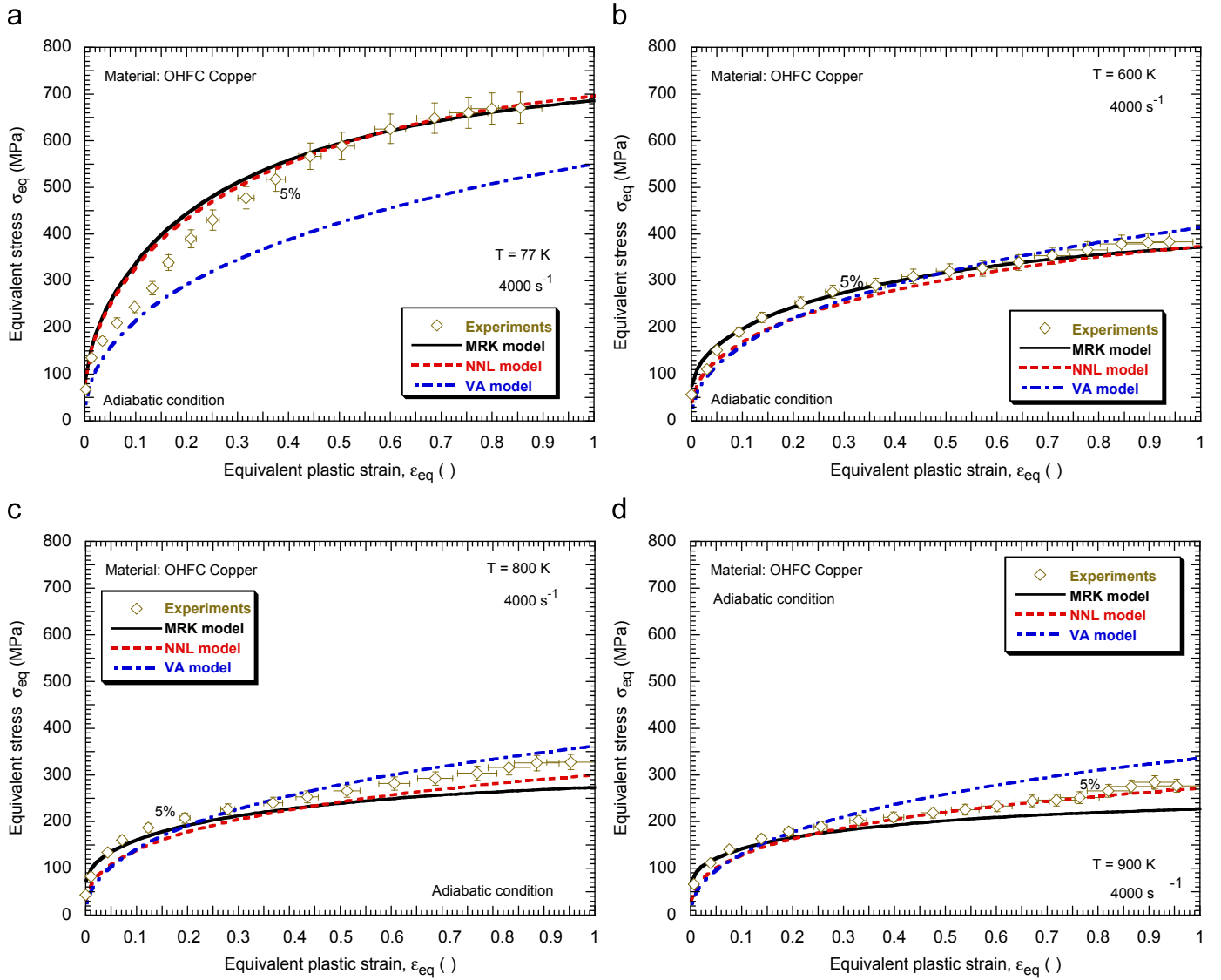
Fig. 16. Description of the flow stress evolution with plastic strain using the **MRK**, **NNL** and **VA** models and comparison with experiments at 4000 s^{-1}: (a) T_0 77 K, (b) T_0 600 K, (c) T_0 800 K and (d) T_0 900 K [8].
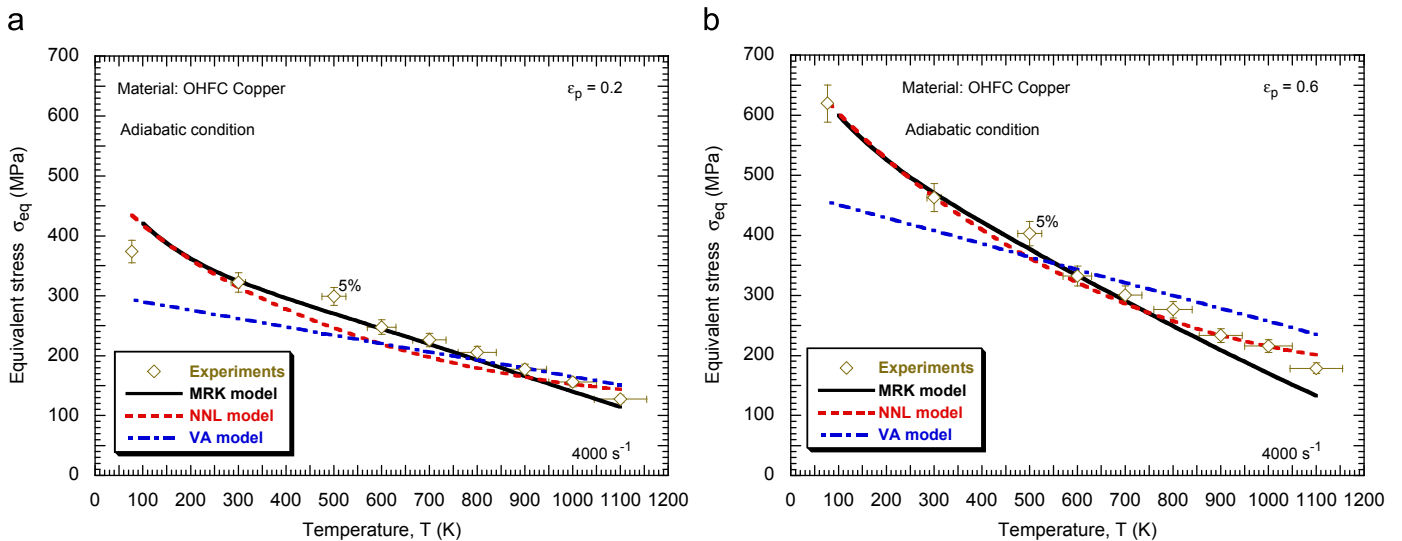

Fig. 17. Temperature sensitivity description using the **MRK**, **NNL** and **VA** models and comparison with experiments at 4000 s^{-1}: (a) ε^p 0.2 and (b) ε^p 0.6 [8].
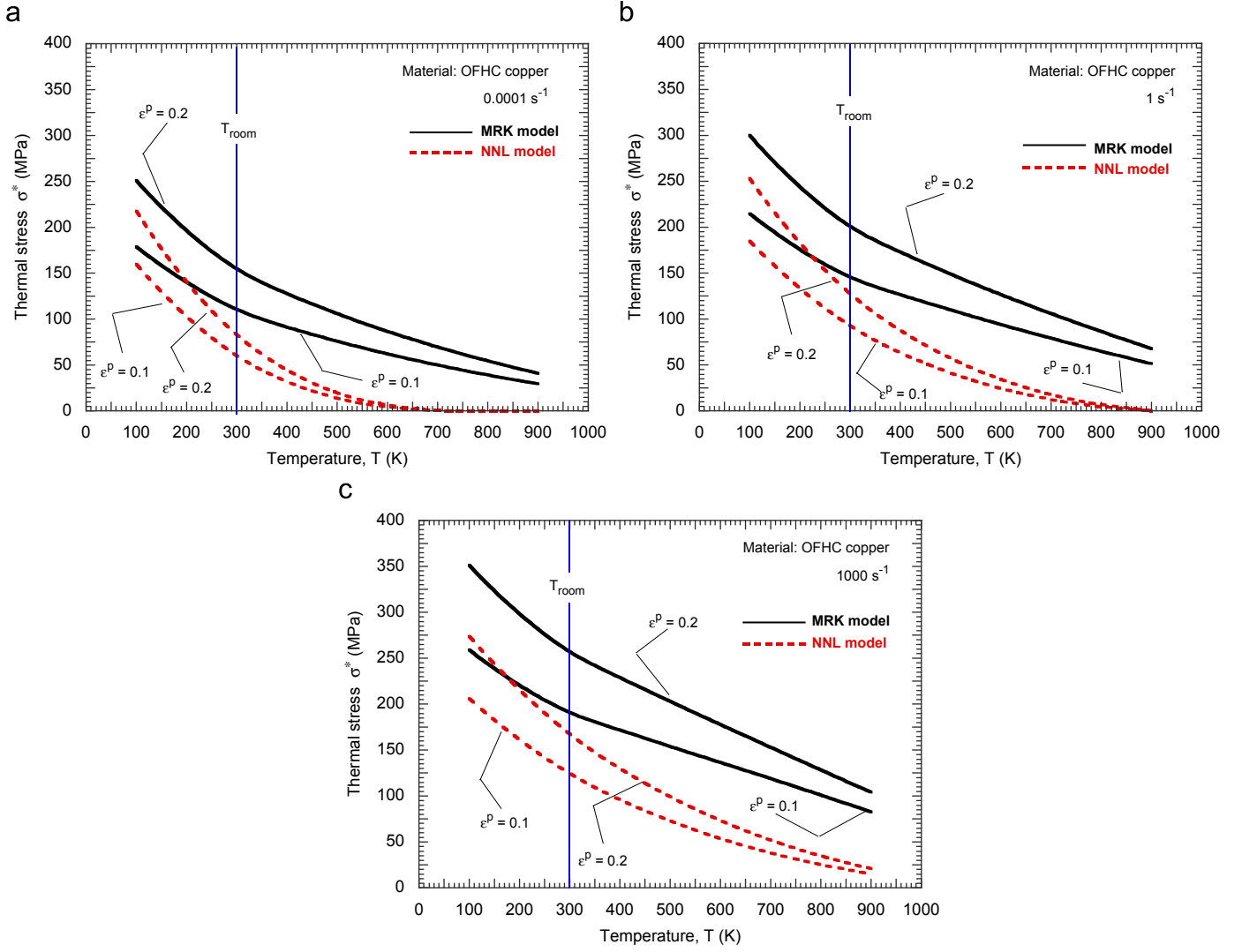
Fig. 18. Evolution of the effective stress σ^* with temperature using the **MRK** and **NNL** models for two deformation levels ε^p 0.1 and ε^p 0.2: (a) 0.0001, (b) 1 and (c) 1000 s ^{1}

Appendix A

A.1. Three dimensional model

As reported, for example, in [59] generalization of constitutive relations to three dimensional (3D) states of stress and strain has particular relevance. For this, the constitutive description intro duced in this paper may be extended to 3D modeling and implemented into **FE** codes by means, for example, of the integration scheme proposed in [60]. This procedure has been already applied to the formulation of the **RK** model [61]. Thus, the main features of the algorithm proposed by Zaera and Fernández Sáez [60] are described below.

The yield condition is defined by

$$f = \overline{\sigma} \quad \sigma_y(\overline{\varepsilon}^p, \dot{\overline{\varepsilon}}^p, T) = 0 \tag{A.1}$$

where $\overline{\sigma}$ is the equivalent stress, σ_y the yield stress defined by the **MRK** constitutive description, $\overline{\varepsilon}^p$ the equivalent plastic strain (Eq. (A.3)), $\dot{\overline{\varepsilon}}^p$ the equivalent plastic strain rate (Eq. (A.3)) and T the temperature:

$$\dot{\overline{\varepsilon}}^p = \sqrt{\frac{2}{3} \dot{\varepsilon}_{ij}^p \dot{\varepsilon}_{ij}^p} \tag{A.2}$$

$$\overline{\varepsilon}^p = \int \dot{\overline{\varepsilon}}^p \, dt \tag{A.3}$$

Assuming additive decomposition of the deformation tensor (*hypoelastic plastic approach*), the tensor of total strain rate $\dot{\varepsilon}_{ij}$ is written as a sum of the elastic strain rate tensor $\dot{\varepsilon}_{ij}^e$, the plastic

13

strain rate tensor $\dot{\varepsilon}_{ij}^p$ and the thermal strain rate tensor $\dot{\varepsilon}_{ij}^T$:

$$\dot{\varepsilon}_{ij} = \dot{\varepsilon}_{ij}^e + \dot{\varepsilon}_{ij}^p + \dot{\varepsilon}_{ij}^T \tag{A.4}$$

Elastic strains are related to stress through an isotropic hypoelastic law:

$$\dot{\sigma}_{ij} = C_{ijkl}\varepsilon_{kl}^e \tag{A.5}$$

where C_{ijkl} is the stiffness tensor.

The thermal strains tensor is defined as follows:

$$\varepsilon_{ij}^T = \alpha \dot{T} \delta_{ij} \tag{A.6}$$

where α is the coefficient of thermal expansion and δ_{ij} the unit matrix ($\delta_{ij} = 1$ if $i = j$).

To define the plastic flow, the normality rule is used:

$$\varepsilon_{ij}^p = \dot{\lambda}\frac{\partial f}{\partial \sigma_{ij}} \tag{A.7}$$

where $\dot{\lambda}$ is the rate plastic multiplier that, in J2 plasticity, can be defined by

$$\dot{\lambda} = \frac{\Delta\lambda}{\Delta t} = \dot{\bar{\varepsilon}}^p \tag{A.8}$$

and hence, the equivalency of the plastic multiplier and the equivalent plastic strain:

$$\bar{\varepsilon}^p = \lambda \tag{A.9}$$

Adiabatic conditions of deformation are assumed (Eq. (14)).

The consistency model is used to integrate the thermo viscoplastic rate equations, via the equality of equivalent stress and yield stress for updated values of plastic strain, plastic strain rate and temperature. In the frame of the return mapping algorithms, the consistency condition, Eq. (A.10), can be written in terms of the equivalent plastic strain increment corresponding to a time step (Eq. (A.11)):

$$\dot{\lambda}f = 0 \tag{A.10}$$

$$f(\Delta\bar{\varepsilon}^p) = 0 \tag{A.11}$$

Linearising the consistency condition, the following equation is found, which allows us to iteratively obtain $\Delta\bar{\varepsilon}^p$:

$$f_{(k+1)} \approx f_{(k)} + \frac{\partial f}{\partial \sigma_{ij}}\left(\delta\bar{\varepsilon}_{(k)}^p 2G\frac{\partial f}{\partial \sigma_{ij}}|_{(k)}\right) + \frac{\partial f}{\partial \bar{\varepsilon}^p}|_{(k)}\delta\bar{\varepsilon}_{(k)}^p$$
$$+ \frac{\partial f}{\partial \dot{\bar{\varepsilon}}^p}|_{(k)}\frac{\delta\bar{\varepsilon}_{(k)}^p}{\Delta t}$$
$$+ \frac{\partial f}{\partial T}|_{(k)}\frac{\beta}{\rho C_p}(\delta\bar{\varepsilon}_{(k)}^p \overline{\sigma}_{n+1}^{trial} \quad 6G\Delta\bar{\varepsilon}_{(k)}^p \delta\bar{\varepsilon}_{(k)}^p)$$
$$= 0 \tag{A.12}$$

where k is an iterative index. From the previous expression, $\delta\bar{\varepsilon}_{(k)}^p$ can be calculated:

$$\delta\bar{\varepsilon}_{(k)}^p \approx \frac{f_{(k)}}{3G \quad \frac{\partial f}{\partial \bar{\varepsilon}^p}|_{(k)} \quad \frac{1}{\Delta t}\frac{\partial f}{\partial \dot{\bar{\varepsilon}}^p}|_{(k)} \quad \frac{\partial f}{\partial T}|_{(k)}\frac{\beta}{\rho C_p}(\overline{\sigma}_{n+1}^{trial} \quad 6G\Delta\bar{\varepsilon}_{(k)}^p)} \tag{A.13}$$

Then, $\Delta\lambda$ is updated after every iteration:

$$\Delta\lambda_{(k+1)} = \Delta\lambda_{(k)} + \delta\lambda_{(k)} \tag{A.14}$$

All the variables can be determined from the final value of $\Delta\lambda$. A more detailed explanation of the integration procedure can be found in [60].

The derivatives of the yield function in terms of $\bar{\varepsilon}^p$, $\dot{\bar{\varepsilon}}^p$ and T are easily obtained for the proposed hardening model. Thus, the derivatives of the thermal stress are as follows (*the remaining model derivatives are common to those corresponding to the original RK formulation and to the extension of the RK model to viscous drag effects. They can be found in* [17,29]):

$$\frac{d\overline{\sigma}^*(\dot{\bar{\varepsilon}}^p, \bar{\varepsilon}^p, T)}{d\dot{\bar{\varepsilon}}^p}|_{\bar{\varepsilon}^p, T} = \frac{B_0(\bar{\varepsilon}^p)^{n_0\left(1 - \frac{D_2 T \log\left(\frac{\dot{\bar{\varepsilon}}^p}{\dot{\varepsilon}_{min}}\right)}{T_m}\right)} vT\left(1 \quad \frac{T\xi_1 \log\left(\frac{\dot{\varepsilon}_{max}}{\dot{\bar{\varepsilon}}^p}\right)}{T_m}\right)^{1/\xi_2}\left(\frac{T\log\left(\frac{\dot{\varepsilon}_{max}}{\dot{\bar{\varepsilon}}^p}\right)}{T_m}\right)^{-1-v}}{\dot{\bar{\varepsilon}}^p T_m}$$

$$+ \frac{B_0(\bar{\varepsilon}^p)^{n_0\left(1 - \frac{D_2 T \log\left(\frac{\dot{\bar{\varepsilon}}^p}{\dot{\varepsilon}_{min}}\right)}{T_m}\right)} T\xi_1\frac{1}{\xi_2}\left(1 \quad \frac{T\xi_1 \log\left(\frac{\dot{\varepsilon}_{max}}{\dot{\bar{\varepsilon}}^p}\right)}{T_m}\right)^{-1+1/\xi_2}\left(\frac{T\log\left(\frac{\dot{\varepsilon}_{max}}{\dot{\bar{\varepsilon}}^p}\right)}{T_m}\right)^{-v}}{\dot{\bar{\varepsilon}}^p T_m}$$

$$\frac{B_0 D_2(\bar{\varepsilon}^p)^{n_0\left(1 - \frac{D_2 T \log\left(\frac{\dot{\bar{\varepsilon}}^p}{\dot{\varepsilon}_{min}}\right)}{T_m}\right)} n_0 T \log(\bar{\varepsilon}^p)\left(1 \quad \frac{T\xi_1 \log\left(\frac{\dot{\varepsilon}_{max}}{\dot{\bar{\varepsilon}}^p}\right)}{T_m}\right)^{1/\xi_2}\left(\frac{T\log\left(\frac{\dot{\varepsilon}_{max}}{\dot{\bar{\varepsilon}}^p}\right)}{T_m}\right)^{-v}}{\dot{\bar{\varepsilon}}^p T_m} \tag{A.15}$$

$$\frac{d\overline{\sigma}^*(\dot{\overline{\varepsilon}}^p,\overline{\varepsilon}^p,T)}{dT}\Big|_{\overline{\varepsilon}^p,\dot{\overline{\varepsilon}}^p} = \frac{B_0(\overline{\varepsilon}^p)^{n_0\left(1-\frac{D_2 T\log\left(\frac{\dot{\overline{\varepsilon}}^p}{\dot{\varepsilon}_{min}}\right)}{T_m}\right)} v\left(1 \frac{T\xi_1\log\left(\frac{\dot{\varepsilon}_{max}}{\dot{\overline{\varepsilon}}^p}\right)}{T_m}\right)^{1/\xi_2}\log\left(\frac{\dot{\varepsilon}_{max}}{\dot{\overline{\varepsilon}}^p}\right)\left(\frac{T\log\left(\frac{\dot{\varepsilon}_{max}}{\dot{\overline{\varepsilon}}^p}\right)}{T_m}\right)^{-1-v}}{T_m}$$

$$\frac{B_0(\overline{\varepsilon}^p)^{n_0\left(1-\frac{D_2 T\log\left(\frac{\dot{\overline{\varepsilon}}^p}{\dot{\varepsilon}_{min}}\right)}{T_m}\right)}\xi_1\frac{1}{\xi_2}\log\left(\frac{\dot{\varepsilon}_{max}}{\dot{\overline{\varepsilon}}^p}\right)\left(1 \frac{T\xi_1\log\left(\frac{\dot{\varepsilon}_{max}}{\dot{\overline{\varepsilon}}^p}\right)}{T_m}\right)^{-1+1/\xi_2}\left(\frac{T\log\left(\frac{\dot{\varepsilon}_{max}}{\dot{\overline{\varepsilon}}^p}\right)}{T_m}\right)^{-v}}{T_m}$$

$$\frac{B_0 D_2(\overline{\varepsilon}^p)^{n_0\left(1-\frac{D_2 T\log\left(\frac{\dot{\overline{\varepsilon}}^p}{\dot{\varepsilon}_{min}}\right)}{T_m}\right)}n_0\log(\overline{\varepsilon}^p)\left(1 \frac{T\xi_1\log\left(\frac{\dot{\varepsilon}_{max}}{\dot{\overline{\varepsilon}}^p}\right)}{T_m}\right)^{1/\xi_2}\left(\frac{T\log\left(\frac{\dot{\varepsilon}_{max}}{\dot{\overline{\varepsilon}}^p}\right)}{T_m}\right)^{-v}\log\left(\frac{\dot{\overline{\varepsilon}}^p}{\dot{\varepsilon}_{min}}\right)}{T_m} \tag{A.16}$$

$$\frac{d\overline{\sigma}^*(\dot{\overline{\varepsilon}}^p,\overline{\varepsilon}^p,T)}{d\overline{\varepsilon}^p}\Big|_{\dot{\overline{\varepsilon}}^p,T} = B_0\left(\frac{T\log\left(\frac{\dot{\varepsilon}_{max}}{\dot{\overline{\varepsilon}}^p}\right)}{T_m}\right)^{-v}(\overline{\varepsilon}^p)^{n_0\left(1-\frac{D_2 T\log\left(\frac{\dot{\overline{\varepsilon}}^p}{\dot{\varepsilon}_{min}}\right)}{T_m}\right)-1}n_0\left(1 \frac{D_2 T\log\left(\frac{\dot{\overline{\varepsilon}}^p}{\dot{\varepsilon}_{min}}\right)}{T_m}\right)\left(1 \xi_1\left(\frac{T}{T_m}\right)\log\left(\frac{\dot{\varepsilon}_{max}}{\dot{\overline{\varepsilon}}^p}\right)\right)^{1/\xi_2} \tag{A.17}$$

It is necessary to notice that using the consistency model only pure elastic unloading is allowed. This fact causes a difference in comparison with, for example, Perzyna overstress model [62], which leads to plastic deformation during unloading so long as overstress is present.

References

[1] Cowper GR, Symonds PS. Strain hardening and strain rate effects in the impact loading of cantilever beams. Report no. 28, Division of Applied Mechanics, Brown University, 1952.

[2] Litonski J. Plastic flow of a tube under adiabatic torsion. Bull Pol Acad Sci 1977;25:7–14.

[3] Johnson GR, Cook WH. A constitutive model and data for metals subjected to large strains, high strain rates and high temperatures. In: Proceedings of the seventh international symposium on ballistics, 1983. p. 541–7.

[4] Klepaczko JR. A practical stress–strain–strain rate–temperature constitutive relation of the power form. J Mech Work Technol 1987;15:143–65.

[5] El-Magd E. Mechanical properties at high strain rates. J Phys IV 1994;C8(4):149–70.

[6] Kocks UF, Argon AS, Ashby MF. Thermodynamics and kinetics of slip. In: Chalmers B, Christian JW, Massalski TB, editors. Progress in materials science, vol. 19. Oxford: Pergamon Press; 1975.

[7] Zerilli FJ, Armstrong RW. Dislocation-mechanics-based constitutive relations for material dynamics calculations. J Appl Phys 1987;61:1816–25.

[8] Nemat-Nasser S, Li Y. Flow stress of FCC polycrystals with application to OFHC Copper. Acta Mater 1998;46:565–77.

[9] Rusinek A, Klepaczko JR. Shear testing of sheet steel at wide range of strain rates and a constitutive relation with strain-rate and temperature dependence of the flow stress. Int J Plasticity 2001;17:87–15.

[10] Nemat-Nasser S, Guo WG. Thermomechanical response of DH-36 structural steel over a wide range of strain rates and temperatures. Mech Mater 2003;35:1023–47.

[11] Molinari A, Ravichandran G. Constitutive modeling of high-strain-rate deformation in metals based on the evolution of an effective microstructural length. Mech Mater 2005;37:737–52.

[12] Voyiadjis GZ, Abed FH. Microstructural based models for bcc and fcc metals with temperature and strain rate dependency. Mech Mater 2005;37:355–78.

[13] Abed FH, Voyiadjis GZ. Plastic deformation modeling of AL-6XN stainless steel at low and high strain rates and temperatures using a combination of bcc and fcc mechanisms of metals. Int J Plasticity 2005;21:1618–39.

[14] Durrenberger L, Molinari A, Rusinek A. Internal variable modeling of the high strain-rate behavior of metals with applications to multiphase steels. Mater Sci Eng A 2008;478:297–304.

[15] Voyiadjis GZ, Almasri AH. A physically based constitutive model for fcc metals with applications to dynamic hardness. Mech Mater 2008;40:549–63.

[16] Rodríguez-Martínez JA, Rusinek A, Klepaczko JR. Constitutive relation for steels approximating quasi-static and intermediate strain rates at large deformations. Mech Res Commun 2009;4:419–27.

[17] Rusinek A, Rodríguez-Martínez JA. Thermo-viscoplastic constitutive relation for aluminium alloys, modeling of negative strain rate sensitivity and viscous drag effects. Mater Des 2009;30:4377–90.

[18] Rusinek A, Rodríguez-Martínez JA, Zaera R, Klepaczko JR, Arias A, Sauvelet C. Experimental and numerical analysis of failure process of mild steel sheets subjected to perpendicular impact by hemispherical projectiles. Int J Impact Eng 2009;36(4):565–87.

[19] Kocks UF. Realistic constitutive relations for metal plasticity. Mater Sci Eng A 2001;317:181–7.

[20] Kocks UF, Mecking H. Physics and phenomenology of strain hardening: the FCC case. Prog Mater Sci 2003;48:171–273.

[21] Bonora N, Milella PP. Constitutive modeling for ductile behavior incorporating strain rate, temperature, and damage mechanics. Int J Impact Eng 2001;26:53–64.

[22] Nemat-Nasser S, Isaacs J. Direct measurement of isothermal flow stress of metals at elevated temperatures and high strain rates with application to Ta and Ta–W alloys. Acta Metall 1997;45:907–19.

[23] Lennon AM, Ramesh KT. The influence of crystal structure on the dynamic behavior of materials at high temperatures. Int J Plasticity 2004;20:269–290.

[24] Seeger A. The mechanism of glide and work-hardening in face-centered cubic and hexagonal close-packed metal. In: Dislocations and mechanical properties of crystals New York: Wiley; 1957.

[25] Klepaczko JR. Thermally activated flow and strain rate history effects for some polycrystalline FCC metals. Mater Sci Eng 1975;18:121–35.

[26] Follansbee PS, Kocks UF. A constitutive description of the deformation of copper based on the use of the mechanical threshold stress as an internal state variable. Acta Metall 1988;1:81–93.

[27] Conrad H. On the mechanism of yielding and flow in iron. J Iron Steel Inst 1961;198:364.

[28] Rusinek A, Zaera R, Klepaczko JR, Cheriguene R. Analysis of inertia and scale effects on dynamic neck formation during tension of sheet steel. Acta Mater 2005;53:5387–400.

[29] Rusinek A, Zaera R, Klepaczko JR. Constitutive relations in 3-D for a wide range of strain rates and temperatures—application to mild steels. Int J Solids Struct 2007;44:5611–34.

[30] Taylor G. Thermally-activated deformation of bcc metals and alloys. Prog Mater Sci 1992;36:29–61.

[31] Uenishi A, Teodosiu C. Constitutive modelling of the high strain rate behaviour of interstitial-free steel. Int J Plasticity 2004;20:915–36.

[32] Basinski ZS. Thermally activated glide in face-centred cubic metals and its application to the theory of strain hardening. Philos Mag 1959;4:393–432.

[33] Armstrong RW, Campbell JD. The microstructure and design of alloys. In: Proceedings on the third international conference on the strength of metals and alloys, Institute of Metals and the Iron and Steel Institute, Cambridge, 1973. Vol. 1, p. 529.

[34] Follansbee PS. High-strain-rate deformation of FCC metals and alloys. In: Metallurgical applications of shock-wave and high-strain-rate phenomena. p. 451–79.

[35] Zerilli FJ, Armstrong RW. The effect of dislocation drag on the stress–strain behaviour of FCC metals. Acta Metall Mater 1992;40(8):1803–8.

[36] Zhang S, McCormick PG, Estrin Y. The morphology of Portevin–Le chatelier bands: finite element simulation for Al–Mg–Si. Acta Mater 2001;49:1087–94.

[37] Campbell JD, Ferguson WG. The temperature and strain-rate dependence of the shear strength of mild steel. Philos Mag 1970;81:63–82.

[38] Kumar A, Hauser FE, Dorn JE. Viscous drag on dislocations in aluminum at high strain rates. Acta Metall 1968;9(16):1189–97.

[39] Regazzoni G, Kocks UF, Follansbee PS. Dislocation kinetics at high strain rates. Acta Metall 1987;12(35):2865–75.

[40] Kapoor R, Nemat-Nasser S. Comparison between high strain-rate and low strain-rate deformation of tantalum. Metall Mater Trans 1999;31A: 815–823.

[41] Nemat-Nasser S, Guo WG, Kihl DP. Thermomechanical response of AL-6XN stainless steel over a wide range of strain rates and temperatures. J Mech Phys Solids 2001;49:1823–46.

[42] Guo WG, Nemat-Nasser S. Flow stress of Nitronic-50 stainless steel over a wide range of strain rates and temperatures. Mech Mater 2006;38:1090–103.

[43] Rusinek A, Rodríguez-Martínez JA, Klepaczko JR, Pecherski RB. Analysis of thermo-visco-plastic behaviour of six high strength steels. J Mater Des 2009;30:1748–61.

[44] Klepaczko JR, A general approach to rate sensitivity and constitutive modeling of FCC and BCC metals, in: Impact: Effects of Fast Transient Loadings, Rotterdam (1998) 3-35.

[45] Macdougall D. Determination of the plastic work converted to heat using radiometry. Exp Mech 2000;40:298–306.

[46] Guzmán R, Meléndez J, Zahr J, Pérez-Castellanos JL. Determination of the constitutive relation parameters of a metallic material by measurement of temperature increment in compressive dynamic tests. Exp Mech, doi:10. 1007/s11340-009-9223-z.

[47] Oussouaddi O, Klepaczko JR. An analysis of transition from isothermal to adiabatic deformation in the case of a tube under torsion. J Phys IV 1991;Coll. C3(Suppl. III):C3–323 [in French].

[48] Klepaczko JR, Chiem CY. On rate sensitivity of FCC metals, instantaneous rate sensitivity and rate sensitivity of strain hardening. J Mech Phys Solids 1986;34:29–54.

[49] Mimura K, Tomita Y. Constitutive relations of mild steel and titanium at high rates under multiaxial loading condition. J Phys IV, 1991, p. 813.

[50] Tomita Y, Higo T. Plane strain flow localization in tension and compression of thermo-elasto-viscoplastic blocks under high rates of deformation. Int J Mech Sci 1993;35-12:985.

[51] Tomita Y. Flow localizations in plane-strain thermo-elasto-viscoplastic blocks under a high rate of deformation. Mater Sci Eng 1994;2:701–20.

[52] Klepaczko JR. Constitutive modelling in dynamic plasticity based on physical state variables: a review. In: International proceedings on mechanical and physical behaviour of materials under dynamic loading, Les Editions de Physique, Les Ulis, C3/49, 1988. p. 553–60.

[53] Tanner AB, McDowell DL. Deformation, temperature and strain rates sequence experiments on OFHC Cu. Int J Plasticity 1999;15:375–99.

[54] Rosenberg Z, Ashuach Y, Yeshurun Y, Dekel E. On the main mechanisms for defeating AP projectiles, long rods and shaped charge jets. Int J Impact Eng 2009;36:588–96.

[55] Ayisit O. The influence of asymmetries in shaped charge performance. Int J Impact Eng 2008;35:1399–404.

[56] Klepaczko JR, Rusinek A, Rodríguez-Martínez JA, Pecherski RB, Arias A. Modeling of thermo-viscoplastic behaviour of DH-36 and Weldox 460-E structural steels at wide ranges of strain rates and temperatures, comparison of constitutive relations for impact problems. Mech Mater 2009;41:599–621.

[57] Stein DL, Low JR. Mobility of edge dislocations in silicon–iron crystals. J Appl Phys 1960;31:362–9.

[58] Becker R. On the plasticity of amorphous and crystalline solids. Phys Z 1925;26:919–25.

[59] Lubarda VA, Benson DJ, Meyers MA. Strain-rate effects in rheological models of inelastic response. Int J Plasticity 2003;19:1097–18.

[60] Zaera R, Fernández-Sáez J. An implicit consistent algorithm for the integration of thermoviscoplastic constitutive equations in adiabatic conditions and finite deformations. Int J Solids Struct 2006;43:1594–612.

[61] Rusinek A, Zaera R. Finite element simulation of steel ring fragmentation under radial expansion. Int J Impact Eng 2007;34(4):799–822.

[62] Perzyna P. In: Fundamental problems in viscoplasticity, vol. 9. New York: Academic Press; 1966. p. 243–377.